



ELSEVIER

Contents lists available at ScienceDirect

## Deep-Sea Research I

journal homepage: [www.elsevier.com/locate/dsri](http://www.elsevier.com/locate/dsri)

# Mean vertical and horizontal structure of the subtropical circulation in the South Atlantic from three-dimensional observed velocity fields



Claudia Schmid\*

NOAA/AOML/PHOD, 4301 Rickenbacker Causeway, Miami, FL 33149, USA

## ARTICLE INFO

## Article history:

Received 28 October 2013

Received in revised form

22 April 2014

Accepted 29 April 2014

Available online 21 May 2014

## Keywords:

Subtropical gyre

Transport

South Atlantic

Three-dimensional velocity field from observations

## ABSTRACT

An analysis of the mean three-dimensional horizontal circulation in the subtropical South Atlantic based on velocity fields derived primarily from Argo data and AVISO sea surface heights, collected in the years 2000–2012, provides new insight into the zonal and meridional transports in the subtropical gyre. The velocity fields reveal the reduction of the latitudinal extent of the subtropical gyre with increasing depth that is mainly due to a southward shift of the westward flowing branch of the subtropical gyre, which is most pronounced near the western boundary. An analysis of zonal and meridional transports in the subtropical gyre in five 400 m thick layers from the surface to 2000 m reveals an interior pathway from the South Atlantic Current (SAC) to the Southern South Equatorial Current (SSEC) between 18°W and 1°E. At 35°S the northward transport in this longitude band ranges from 5.5 Sv (1 Sv = 1 Sverdrup =  $10^6 \text{ m}^3 \text{ s}^{-1}$ ) in the shallowest layer to 3.5 Sv in the deepest layer, and adds up to total transport of 14.6 Sv in the upper 800 m. Within the uncertainty of the estimated transports, these northward transports are consistent with the east-to-west strengthening of the SSEC in 18°W and 1°E (e.g. 14.2 Sv in the upper 800 m). For the SAC, the change of the transport has the correct sign, but the west-to-east shrinking of the transport is larger than the northward transport, which suggests a transfer of water from the SAC to the Antarctic Circumpolar Current. With respect to the boundary currents that are part of the subtropical gyre, the southward transport of the western boundary current in the upper 2000 m increases from 5.2 Sv at 28°S to 44.2 Sv at 33°S. This is followed by a decrease to 22.2 Sv at 36°S and another increase to 38.7 Sv at 39°S. Further analysis shows that the increase of the transport by 15.2 Sv between 31°S and 33°S is primarily due to the small recirculation cell just east of the Brazil Current that has a northward transport of 13.1 Sv at 35°S in the upper 2000 m. Along the eastern boundary, the transport of the Benguela Current within the upper 1200 m at 35°S is 23.9 Sv, increasing by about 10 Sv between 37°S and 32°S. To the east of this current, the Benguela Poleward Undercurrent can be detected in the velocity and salinity fields derived for the core of the Antarctic Intermediate Water. This current extends as far south as 30°S and potentially even to 33°S.

Published by Elsevier Ltd.

## 1. Introduction

The circulation in the South Atlantic has been studied extensively because it is an important part of the Atlantic Meridional Overturning Circulation (AMOC), which consists of a northward transport of relatively warm and fresh upper ocean water of southern origin across the equator into the northern North Atlantic and a southward transport of relatively cold and salty deep water from the North Atlantic into the South Atlantic. The upper branch of the AMOC carries water northward that enters the South Atlantic via the cold and warm water routes. Water from the

cold water route (McCartney, 1977; Georgi, 1979; Piola and Georgi, 1982) enters the Atlantic in the Antarctic Circumpolar Current via the Drake Passage. Water following the warm water route enters the Atlantic from the Indian Ocean via the Agulhas leakage and rings (Gordon, 1985; Lutjeharms and Gordon, 1987; Lutjeharms and Cooper, 1996). Part of the water coming through the Drake Passage continues northward along the western boundary in the Malvinas Current and meets warmer water of subtropical origin that is carried southward in the Brazil Current. After the confluence of these currents (e.g. Gordon, 1989; Garzoli, 1993) the water flows east in the South Atlantic Current (SAC, e.g. Stramma and Peterson, 1990). The water from the two source regions mixes not only in the Cape Basin (e.g. Boebel et al., 2003) but also in the Southern South Equatorial Current (SSEC) on its way to the tropical South Atlantic (e.g. Gordon, 1986; Rintoul, 1991;

\* Tel.: +1 305 361 4313.

E-mail address: [claudia.schmid@noaa.gov](mailto:claudia.schmid@noaa.gov)

Gordon et al., 1992; Schmitz, 1995). Once the SSEC reaches the western boundary it bifurcates at depth-dependent latitudes and feeds into the northward and southward boundary currents (e.g. Stramma and England, 1999; Boebel et al., 1999).

This study will focus on the circulation in the subtropical gyre of the South Atlantic from the surface down to 2000 m. In preparation for this analysis a time-averaged three-dimensional field of the horizontal velocity was derived from Argo profiles, float trajectories and satellite altimetry observations. The method for combining these data sets is similar to the approach used by Willis (2010). With the availability of this velocity field it is possible to take a closer look at the structure of the flow field as well as the zonal transports in conjunction with the meridional transports in the interior and at the western and eastern boundaries at a higher resolution in the horizontal and the vertical than was possible in earlier studies.

With respect to the zonal transports in the subtropical gyre, it was found that they depend strongly on the longitude. For example, Schmid and Garzoli (2009) reported that the transports of AAIW in the SAC and the SSEC depend on the longitude, while Rodrigues et al. (2010) reported that the transport of the SAC in the upper 1000 dbar at 30°W is significantly larger than at the Greenwich Meridian. In an expansion of earlier results, the dependence of the transports of both currents on the longitude and the depth will be analyzed in more detail in conjunction with the meridional transports in the interior.

Along the western boundary, results from various studies provided some information on how the transport of the Brazil Current varies with latitude (e.g. Stramma, 1989; Zemba, 1991; Rodrigues et al., 2010; Garzoli et al., 2012). The new results provide more details on the transports of this current and their latitude-dependence. Similarly, the new results provide more information on the flow near the eastern boundary, both in terms of transports of the Benguela Current (e.g. Stramma and Peterson, 1989; Gordon et al., 1992; Sloyan and Rintoul, 2001; Garzoli et al., 2012) and of the meridional extent of the Benguela Poleward Undercurrent (e.g. Richardson and Garzoli, 2003; Lass and Mohrholz, 2008; Veitch et al., 2010).

Overall, the results of this study improve the knowledge of the flow patterns in this region and will be helpful for model validation. In addition, the time series of monthly three-dimensional velocity fields that was used to derive the climatological mean provides, for example, an opportunity to use them for efforts related to the observation and monitoring of the AMOC from the time on when the data coverage is sufficient using methods similar to those developed in other studies (e.g. Baringer and Garzoli, 2007; Garzoli and Baringer, 2007; Hobbs and Willis, 2012). While this study includes an analysis of meridional transports within the region governed by the subtropical gyre, an estimation of the total transport of the AMOC is beyond the scope of this study.

The paper is organized as follows. In Section 2 the data sets and the methodology for the derivation of the mean three-dimensional flow field are described. Section 3 focuses on the depth-dependence of the flow. The longitude-dependence of the zonal currents in the context of the circulation in the subtropical gyre will be addressed in Section 4. Section 5 summarizes the results.

## 2. Data and methodology

Three data sets are used herein to derive the absolute three-dimensional geostrophic velocity field. These data sets are profiles of temperature and salinity, subsurface velocities from float trajectories and sea surface heights. In addition, wind fields are needed to estimate the Ekman velocity that needs to be added to the geostrophic velocity prior to studying the circulation. Where

these data sets come from and how they are used is described in the following.

The temperature and salinity profiles covering the years 2000–2012 come from an array of roughly 3000 floats that drift freely in the world ocean as part of the Argo project (the goal of 3000 active floats was reached in 2007). These data were obtained from one of the Argo Global Data Assembly Centers.<sup>1</sup> All profiles from Argo floats pass through a series of automatic quality control procedures in real-time. A document describing these tests is available online.<sup>2</sup> To facilitate the detection of sensor drifts in real-time profiles collected by the US Argo Data Assembly Center (Schmid et al., 2007), the profiles are also compared with the NCEP ocean reanalysis (Global Ocean Data Assimilation System, GODAS, Saha et al., 2005) and the World Ocean Atlas (Antonov et al., 2006; Locarnini et al., 2006). In delayed-mode a scientific quality control of Argo profiles is performed that aims at improving the value of the flags assigned by the automatic quality control tests, as well as at correcting a potential drift of the salinity sensor. In this study, bad measurements with a quality control flag that is not one are excluded in all profiles. In the next step, profiles that have gaps exceeding 100 dbar or do not have enough levels with good data are excluded. The number of profiles with temperature and salinity collected in the study region (Fig. 1) in the thirteen years (2000–2012) since the start of Argo that could be used herein is 59,350. Of these profiles about 74% went through the Argo delayed-mode process. Profile data are available throughout most of the South Atlantic (Fig. 1a) and this data coverage does not depend on the calendar month (not shown).

The trajectory data used for the estimation of the subsurface velocity are from Argo and WOCE floats that were active in January 24, 1990 to March 24, 2013. The float trajectories from before the year 2000, most of which are from acoustically tracked floats, were included to improve the spatial coverage. Trajectories from 1352 floats passed through the study region and 651 of them drifted in the pressure range of 800–1100 dbar. The latter was chosen because it has the largest number of observations. The 651 trajectories are used to derive the velocity field for the level of known motion approach (see below). For all of them, statistical methods based on standard deviations and speed checks are used in conjunction with visual inspections to eliminate bad positions and velocity estimates. As for the profiles, the coverage of the study region with high-quality velocities from the float trajectories is quite good (Fig. 1b) and the data coverage does not depend on the calendar month (not shown). Areas with Argo profiles that have no velocities from the trajectories exist, because some floats did not report the drift pressure for various reasons while other floats drifted outside of the pressure range used in this study (as noted above: only about half of the existing trajectories could be used).

In addition two more data sets are used. One data set contains sea surface height fields from AVISO (provided by CLS, 1996, France, CLS, 1996). The weekly data set of SSALTO/DUACS delayed-time absolute dynamic topography on a 1/4 degree grid downloaded for this study covers the time period January 2000 to June 2012. The other data set consists of wind fields from the NCEP reanalysis 2 (Kanamitsu et al., 2002). How all of the above data sets are used to estimate the three-dimensional fields of the horizontal velocity is presented in the following.

The dynamic height is calculated directly from temperature and salinity profiles as well as indirectly from the sea surface height

<sup>1</sup> Two Argo Global Data Assembly Centers exist: The one in the USA is hosted by the Global Ocean Data Assimilation Experiment ([www.usgodae.org/argo/argo.html](http://www.usgodae.org/argo/argo.html)) and the one in France is operated by Coriolis ([www.coriolis.eu.org/cdc/argo.htm](http://www.coriolis.eu.org/cdc/argo.htm)).

<sup>2</sup> <http://www.argodatamgt.org/Documentation>.

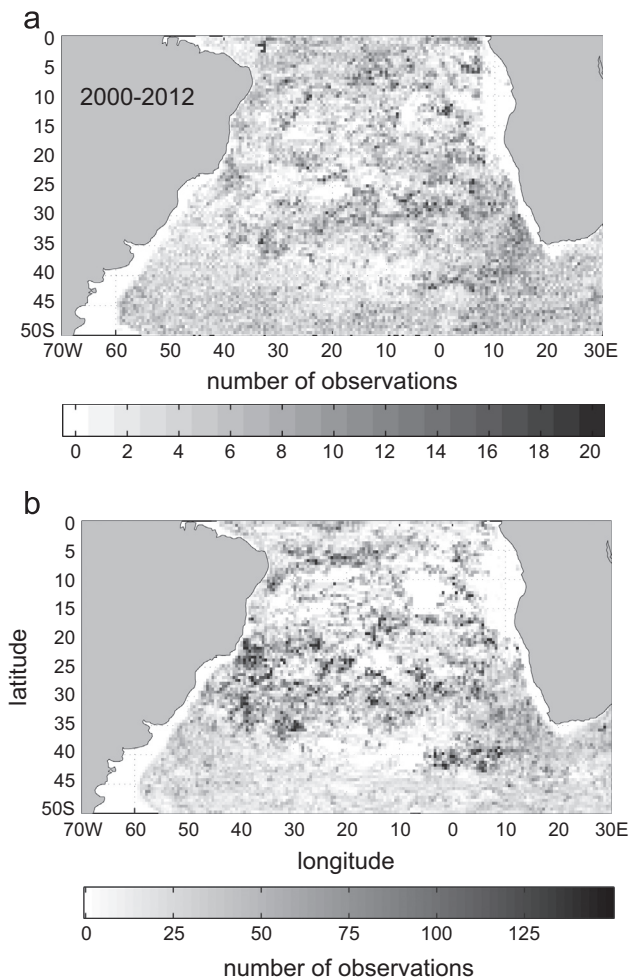


**Fig. 1.** Maps of the data coverage: (a) Availability of Argo profiles with temperature and salinity in the study region for observations collected in the years 2000–2012. (b) Availability of trajectory observations in the study region for observations collected in to January 24, 1990 to March 24, 2013. The bin sizes are  $0.5^\circ$  by  $0.5^\circ$ .

fields for each month and year in the period January 2000 to June 2012 (see Appendix A). Both sets of dynamic height fields are then used to estimate the zonal and meridional geostrophic velocity fields relative to a level of no motion at 1000 dbar, which ultimately results in one set of velocity fields (see Appendix B). To get absolute geostrophic velocities, fields of the subsurface velocity from float trajectories are derived and then used to adjust the relative geostrophic velocity (see Appendix C). Small gaps in the velocity fields are filled using the approach described in Appendix D. Finally, the Ekman velocity fields are calculated and added to the adjusted geostrophic velocity fields using the wind fields mentioned above (see Appendix E). A comparison of a climatological field of the horizontal velocities at a depth of 15 m with independent estimates based on surface drifters drogued at that depth reveals a good agreement between them (see Appendix F). The same is the case for localized comparisons of the velocity at intermediate depth derived herein with those published in earlier studies (see Appendix F).

The derived velocity fields are used to calculate the total zonal and meridional volume transports which are then integrated in the vertical over slabs with thicknesses selected to facilitate studying the changes of the circulation patterns as a function of depth. Climatological fields of the zonal and meridional volume transports are estimated by averaging the monthly fields from the period January 2000 to June 2012.

### 3. Vertical structure

Maps of the climatological transports for layers with varying thicknesses in the upper 400 m of the ocean are shown in Fig. 2a–d while Fig. 2e–h displays the transports in 400 m thick layers from 400 m down to 2000 m. The layers in Fig. 2b–d were chosen to resolve the structure of the circulation in the upper 400 m in more detail because large vertical gradients of the velocity can be expected in many regions. In addition, Fig. 2a,b show the transports in the upper 100 m with and without the Ekman component of the flow. Below 400 m, a constant layer thickness was chosen because it makes it easier to detect reductions of the transport with increasing depth. The way these layers were chosen has the added benefit that the 800–1200 m layer agrees well with the depth where the Antarctic Intermediate Water (AAIW) circulates in the subtropical gyre. In the following, the circulation in the different layers is analyzed based on these estimated transports.

#### 3.1. The 0–100 m layer

As mentioned above, Fig. 2a shows the transport in the upper 100 m without the Ekman transport, while Fig. 2b displays the transport in the same layer with the Ekman transport included. A comparison of these two flow fields reveals that the addition of the Ekman transport has a large impact on the direction and strength of the meridional transport north of  $20^\circ\text{S}$ . Closest to the equator, at  $5^\circ\text{S}$ , the main impact is to make the flow much more zonal than without the Ekman component. In the northeast corner, the cyclonic flow of the Angola Gyre (e.g. Gordon and Bosley, 1991; Stramma and Schott, 1999) with its center at about  $13^\circ\text{S}$ ,  $5^\circ\text{E}$  can be seen clearly in the map of the geostrophic transport (Fig. 2a), while the addition of the Ekman transport masks this gyre (Fig. 2b). South of  $20^\circ\text{S}$ , the addition of the Ekman component only yields relatively small changes of the meridional transport. These differences are too small to have a significant impact on the large-scale spreading of water in the subtropics.

The major zonal currents in this layer are the eastward Antarctic Circumpolar Current (ACC) near the southern edge of the domain, the eastward South Atlantic Current (SAC) around  $40^\circ\text{S}$ , and the Southern South Equatorial Current (SSEC) that is heading from the northern Cape Basin near the tip of South Africa (the southern part of the Cape Basin is marked by CB in Fig. 2a) to the western boundary region, where the high-velocity core can be seen between  $10^\circ\text{S}$  and  $20^\circ\text{S}$  (Fig. 2a). The southern edge of the SSEC current is marked by the solid black line between  $30^\circ\text{S}$  and  $40^\circ\text{S}$ . Within the area dominated by the SSEC is an area of weak eastward flow centered at about  $24^\circ\text{S}$ ,  $40^\circ\text{W}$  (encircled by a black contour line), which corresponds to the eastward flow in the small northern cell of the subtropical gyre described by Vianna and Menezes (2011) in their discussion of the double-celled structure of the subtropical gyre. They found this northern cell between  $21^\circ\text{S}$  and  $27^\circ\text{S}$ , west of  $32^\circ\text{W}$  and the southern cell south of  $28^\circ\text{S}$ , with the largest westward flow between  $28^\circ\text{S}$  and  $32^\circ\text{S}$  (depending on the longitude), which is consistent with the results presented herein. About  $20^\circ$  farther south, between the SAC and the ACC, the anticyclonic Zapiola eddy is clearly visible with its center near  $45^\circ\text{S}$ ,  $45^\circ\text{W}$  (e.g. Volkov and Fu, 2008). More information on this eddy is given in Section 3.4.

With respect to the meridional currents, one can see the southwestward flow of the Brazil Current, with some gaps because this current is very close to the western boundary and thus under-sampled by the floats, and the northwestward flow of the Malvinas Current along the western boundary. These currents meet each other in the Brazil–Malvinas Confluence near  $39^\circ\text{S}$ , which is consistent with earlier observations (e.g. Gordon and Greengrove, 1986; Bianchi and Garzoli, 1997; Gonzalez-Silvera et al., 2006;

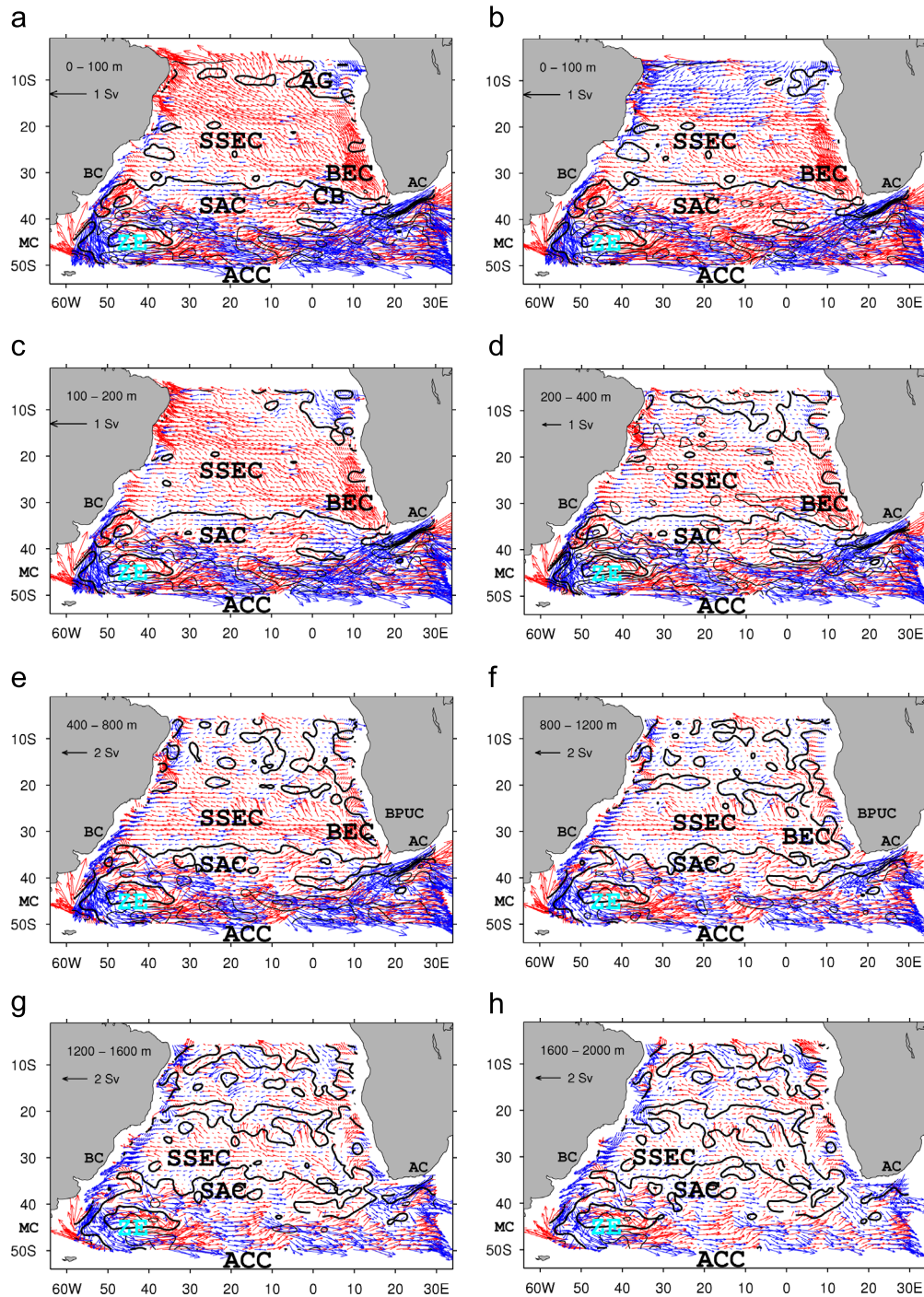


**Fig. 2.** Maps of the adjusted climatological transports ( $1 \text{ Sv} = 10^6 \text{ m}^3 \text{ s}^{-1}$ ). Panels (b) and (c) include the Ekman component. Red (blue) vectors indicate northward (southward) flow. Thick (thin) black lines mark a zonal transport of 0 Sv (0.5 Sv and 1 Sv). Only a subset of the data is shown in the interior (on a  $1^\circ$  by  $1.5^\circ$  grid). AC: Agulhas Current; ACC: Antarctic Circumpolar Current; AG: Angola Gyre; BC: Brazil Current; BEC: Benguela Current; BPUC: Benguela Poleward Undercurrent; SAC: South Atlantic Current; SSEC: Southern South Equatorial Current; ZE: Zapiola Eddy; CB: Cape Basin. (For interpretation of the references to color in this figure caption in black-and-white copies, the reader is referred to the web version of this paper.)

Lumpkin and Garzoli, 2011). The Brazil Current originates in the tropics (at the bifurcation of the SSEC) while the Malvinas Current is fed by water originating in the Drake Passage that is entering the domain in the southwestern corner as a northwestward current that turns northward and then northeastward as it follows the topography. In the southeastern part of the domain one can see the southwestward Agulhas Current as large blue vectors that mask its retroflexion due to the strength of the transport. Along the west coast of Africa the Benguela Current shows itself as a broad northerly transport that mostly feeds into the SSEC. In the interior of the subtropical gyre,

there is a broad area with northward flow approximately between the Greenwich Meridian and  $20^\circ\text{W}$ . This subtropical circulation pattern is in general agreement with earlier results (e.g. Reid, 1989; Stramma and England, 1999).

### 3.2. The 100–200 m layer

In the 100–200 m layer (Fig. 2c), the circulation in most of the domain looks very similar to that in the shallowest layer (Fig. 2b), however, there are three main changes in the northern half of the

domain: (1) the area of weak eastward flow centered at about 24°S, 40°W that exists in the 0–100 m layer and is associated with the double-celled subtropical gyre (see above) is almost completely gone in the 100–200 m layer. (2) The Angola Gyre (e.g. Gordon and Bosley, 1991; Stramma and Schott, 1999) is weaker, but it is still centered at about 13°S, 5°E in the 100–200 m layer (Fig. 2a and c). (3) The 100–200 m layer has significantly fewer vectors with a southward component of the transport northwest of 25°S and the Greenwich Meridian than the 0–100 m layer. The reason for this is that the meridional component of transport due to the Ekman balance is southward in the 0–100 m layer in this region, which can be seen clearly when comparing Fig. 2a and b.

### 3.3. The 200–400 m layer

In the 200–400 m layer (Fig. 2d) the SSEC does not extend as far north as in the two shallower layers, as indicated by a southward shift of the maximum of the transport west of 20°W from north of 15°S to south of 15°S (in Fig. 2c relatively large red vectors can be seen northeast of 15°W, 20°W in an area where smaller velocities of varying zonal flow direction are visible in Fig. 2d). This shift goes hand in hand with a southward shift with increasing depth of the bifurcation of the SSEC into the northward flowing North Brazil Current and southward flowing Brazil Current consistent with earlier studies (e.g. Stramma and England, 1999; Boebel et al., 1999). Farther north, near 10°S, an area of eastward flow (encircled by a thick black contour line) can be seen between 30°W and 5°W in the 200–400 m layer which is in a region that was dominated by westward flow in both shallower layers. Simultaneously, a wide area around this latitude range is governed by southward meridional transports in the 200–400 m layer, while the meridional transport is predominantly northward in the 100–200 m layer. Most likely, a meandering of the flow causes the characteristics in the deeper layer. Farther east, the Angola Gyre (e.g. Gordon and Bosley, 1991; Stramma and Schott, 1999) is centered a bit farther southwest, at about 15°S, 3°E, than in the upper two layers.

### 3.4. Layers below 400 m in comparison with the upper layers

Fig. 2e–h shows the transports in four 400 m thick layers between 400 and 2000 m. As expected, the figure reveals that the transports of the ACC, the SAC and the SSEC decrease with increasing depth. This decrease is stronger in the SAC than in the ACC, which is consistent with earlier results (e.g. Stramma and Peterson, 1990). The vertical shear in the Zapiola eddy is even smaller than in the ACC consistent with results from a previous study of Dewar (1998) that attributed the phenomenon to an eddy-driven flow controlled by bottom friction. An extensive analysis of the dynamics of this eddy can be found in Volkov and Fu (2008).

The area dominated by westward flow in the SSEC decreases with increasing depth. In the upper 400 m, this decrease is reflected in the build-up of a regime with eastward flow in the northeast corner of the domain that expands westward to the point of extending almost all the way from the eastern to the western boundary in 200–400 m (Fig. 2d). This area with alternating patches of eastward and westward flow expands southward with increasing depths (see 400–800 m and deeper layers in Fig. 2e–h). At larger depths an almost completely connected band of eastward flow at about 20°S becomes evident in 800–1200 m (Fig. 2f) and is well-formed in the deepest two layers (1200–1600 m and 1600–2000 m, Fig. 2g and h). Because of this the SSEC at intermediate depth is predominantly zonally oriented, rather than heading west-northwestward as is the case at shallower depths. When comparing the deeper layers with the 0–400 m layer (in which the structure of the SSEC is qualitatively similar to

that in the 0–100 m layer shown in Fig. 2b), these changes yield a 10° smaller latitudinal extent of the gyre in the 800–1200 m layer (Fig. 2f). Below 1200 m (Fig. 2g and h) the latitudinal extent is 15° smaller than in the 0–400 m layer. These characteristics agree quite well with the flow patterns derived in earlier studies (e.g. Reid, 1989; Stramma and England, 1999; Schmid et al., 2000), while providing more details about both the horizontal and the vertical structure.

In addition, the transports in the SSEC become smaller with increasing depth, and the westward transport in the deepest three layers does not start near 15°E, but about 2° farther west. The latter fact means that the Agulhas Leakage is not likely to bring significant amounts of water originating in the Indian Ocean into the northern part of the South Atlantic at these depths. This is consistent with results from earlier studies looking at the vertical structure of the Agulhas Current and the exchange of water between the Indian and the Atlantic Oceans (e.g. Lutjeharms and Cooper, 1996).

As in the shallower three layers (Fig. 2b–d), the northward flow of the Benguela Current is clearly visible near the eastern boundary in the 400–800 m (Fig. 2e) and the 800–1200 m layers (Fig. 2f). Different from the flow field in the shallower layers is the fact that areas of southward flow are present farther east, between the Benguela Current and the coast of Africa. These are associated with the Benguela Poleward Undercurrent. More information on this current follows in Section 4.3.1.

## 4. Longitude-dependence of zonal transports in the subtropical gyre

### 4.1. The South Atlantic Current

To estimate the total zonal transports of the SAC in each layer the boundaries of this current were defined as follows. The northern boundary is the latitude where the flow direction changes from eastward to westward (thick black line crossing the basin near 30°S in Fig. 2), while the southern boundary is the location of the Subtropical Front approximated as the latitude of minimum zonal transport that is closest to the latitude where the salinity in the mixed layer is 34.9 psu (Deacon, 1982). Once the boundaries of the current have been determined the transport in 400 m thick layers is derived for each month in all years. The resulting transports and the latitudinal boundaries are used to estimate their climatological means as well as their standard deviations. The left panels in Fig. 3 show the zonal transports while the right panels show the meridional boundaries for each 400 m thick layer. Below 800 m, the transport estimates east of the Greenwich Meridian are less robust, because it is more difficult to determine the northern and southern boundaries of this current in that region. The reason for this is the high variability governing the circulation in the Cape Basin.

The left panels in Fig. 3 reveal a pronounced longitude-dependence of the zonal transports of the SAC in all 400 m thick layers between the surface and 2000 m. In the interior, this is reflected in a significant west to east decrease of the transport between 22°W and 7°E. In terms of the vertical structure the large transports found near 22°W decrease from 32.4 Sv in the shallowest layer (Fig. 3, top left) to 11.9 Sv in the deepest layer (Fig. 3, bottom left). The magnitude of the transport reduction between layers decreases with increasing depth, which is consistent with the larger vertical shear of the zonal velocity in the upper ocean than at intermediate depths. The minimum of the zonal transport found near 7°E ranges from 8.4 Sv (upper layer) to 0.4 Sv (in 800–1200 m) and is 1.1 Sv in the two deepest layers. The differences between the interior minimum and maximum decrease from

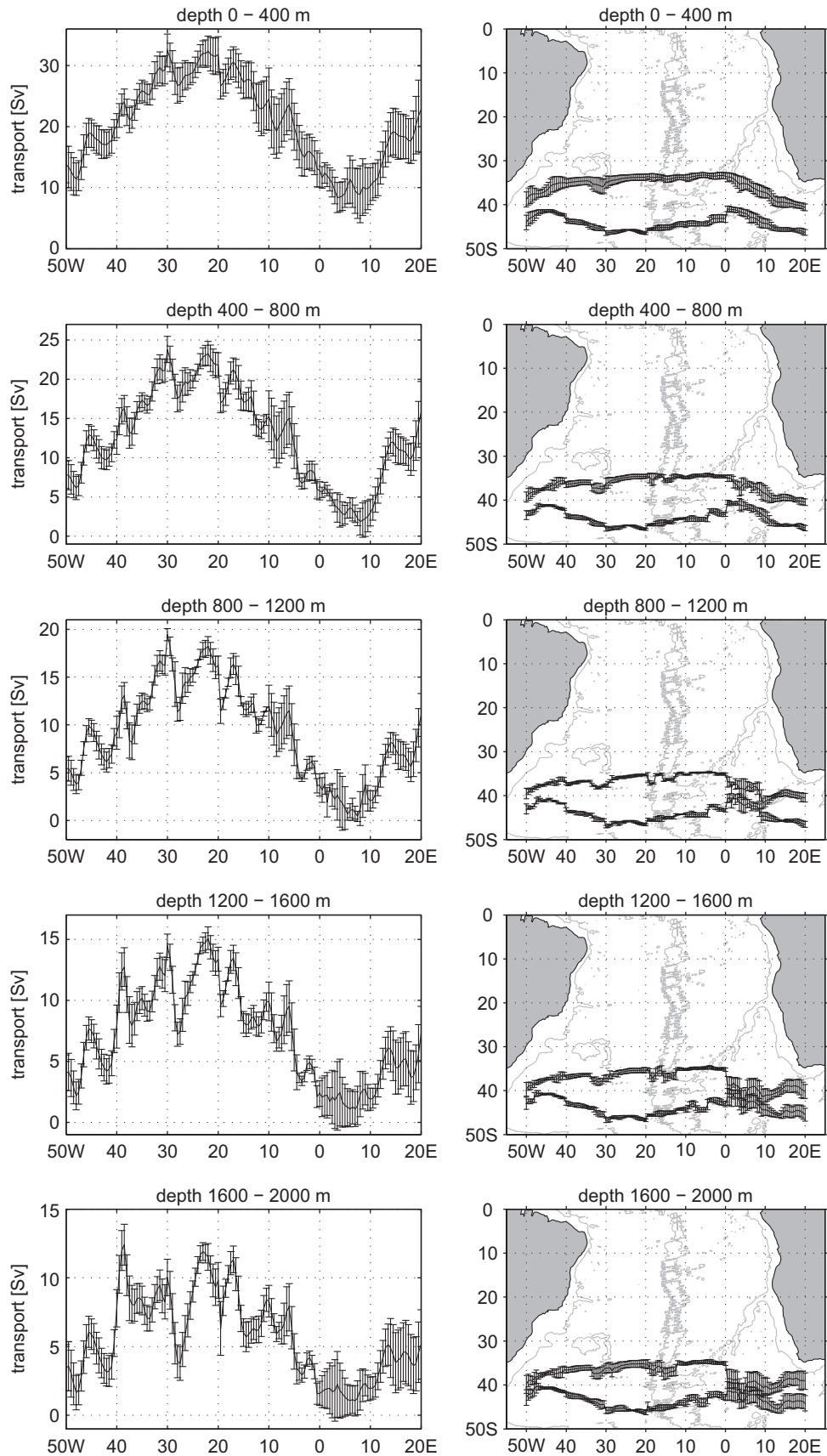


**Fig. 3.** Climatological zonal transport as a function of longitude (left) and maps depicting latitude limits (right) for the South Atlantic Current as derived from the monthly estimates from all years. Error bars indicate the standard deviation. The right panels show the 3500 m isobath.

24.0 Sv in 0–400 m to 21.4 Sv in 400–800 m, 17.8 Sv in 800–1200 m, 14.0 Sv in 1200–1600 m and 10.8 Sv in 1600–2000 m. As mentioned above, the uncertainty of the transports in the deepest layer is relatively large east of the Greenwich Meridian because it is more difficult to define the boundaries of the SAC there. However, the impact of this uncertainty on the magnitude of the west to east decrease of the transports is quite small because the large transports near 22°W dominate the signal.

The longitude-dependence of the transports is partly due to a change in the width of the current. In the interior the latitude of the northern edge of the current does not depend much on the longitude. Mainly, it shifts southward east of the Greenwich Meridian and west of about 40°W (Fig. 3, right panels). A stronger and more complex longitude-dependence of the southern edge of the current can be discerned in all layers. A southward shift between 45 and 20°W is followed by a weaker northward shift between 20°W and the Greenwich Meridian. East of the Greenwich Meridian, there is another weak southward shift. For both, the northern and the southern boundary of the current, the standard deviations east of the Greenwich Meridian are larger than west of it. Overall, there is a tendency towards larger transports where the current is wider. This is reflected in correlations between the transport and the width of the current that are quite large, with values of about 0.78 in the upper four layers and 0.73 in the deepest layer. A discussion on the challenges of defining the latitudinal boundaries of this current as well as an interpretation of the transport changes follows in Section 4.4.

In the following, the reduction of the transport between 30°W and the Greenwich Meridian will be derived to allow a comparison of the longitude-dependence of the transport with earlier results. Because the transports at both longitudes not only vary with time but also depend on the longitude itself, means and standard deviations are derived within 2° of each of the two longitudes. In 28–32°W this approach results in mean transports of about 50 Sv in the upper 800 m and about 67 Sv in the upper 1200 m, with standard deviations of 5 Sv and 7 Sv, respectively. Within 2° of the Greenwich Meridian the transports are 20 Sv in the upper 800 m and 25 Sv in the upper 1200 m with standard deviations of 4 Sv and 5 Sv, respectively. Based on these transports the west to east decreases of the transport are 60% in the upper 800 m and 62% in the upper 1200 m.

A study based on several hydrographic sections across the SAC by Stramma and Peterson (1990) reported that the SAC transport in the upper 1000 m decreases from west to east by 59% (from 37 Sv at 30°W to about 15 Sv at the Greenwich Meridian, based on a level of no motion in the depth range of 2900–3600 m). In a more recent study, Rodrigues et al. (2010) also reported a reduction of the transport of this current in the upper 1000 m by about 60% for the same longitude range (from 50 Sv to 19 Sv, barotropic transport included). In contrast to this, transports in the upper 1500 m derived by Smythe-Wright et al. (1998) indicate that the west to east decrease in this longitude range is only 24% (from 37.0 Sv to 28.2 Sv, based on a level of no motion at 1500 m). Two factors are likely to give rise to this small reduction: (1) the barotropic component of the flow is important for estimating the transport of the SAC and (2) potentially their transport estimate for the Greenwich Meridian includes the eastward flow south of 40°S that is separated from the SAC by a wide band of westward flow and thus is not likely to be part of the SAC. The new reductions derived herein agree quite well with the result of Rodrigues et al. (2010) as well as the higher percentage from Stramma and Peterson (1990), while all these estimates are significantly larger than the estimate of Smythe-Wright et al. (1998).

The transport in the 800–1200 m layer, which is roughly representative of the AAIW layer, can be compared to results of Schmid and Garzoli (2009) for this water mass. The focus will be

on the transports at the maximum (at 30°W) and the minimum (at 7°E) as well as the west to east decrease of the transports. Because the transports vary quite strongly within 2° of both longitudes, a more detailed analysis is done to determine the mean and its uncertainties. The mean of all transports derived in the longitude range 28–32°W is 16.3 Sv with a standard deviation 2.3 Sv.<sup>3</sup> For the longitude range of 5–9°E, the overall mean and standard deviation are 1.3 Sv and 1.7 Sv, respectively.<sup>4</sup> The difference between the two overall means of 16.3 Sv and 1.3 Sv results in a west to east decrease of 15.0 Sv with an uncertainty on the order of 4 Sv. Schmid and Garzoli (2009) found that the transport of the SAC at the depth of the AAIW, between 800 and 1100 dbar, is 5.5 Sv at 30°W and 0.0 Sv at 7°E (the corresponding standard deviations do not exceed 1.1 Sv). When adjusting these earlier estimates to be representative for a 400 m thick layer, then the transport difference between the two longitudes is about 7.3 Sv. In addition, the southern boundary used for the transport estimates by Schmid and Garzoli (2009) is farther north while having a similar shape, which results in a 40% narrower SAC.<sup>5</sup> Correcting for this difference of the width of the current increases the transport estimated by Schmid and Garzoli (2009) to 10.2 Sv. In the light of the statistical characteristics and the method-based differences of the two independent estimates of the transport, about 15 Sv for the new result versus about 10 Sv for the earlier result can be seen as consistent with each other. Overall, the comparisons with the previous studies show that the new velocity fields represent the longitude-dependence of the SAC very well and thus can be used to study this characteristic in more detail both on the vertical and zonal axis.

#### 4.2. The Southern South Equatorial Current

For each of the monthly fields available in the twelve years considered in this study, the SSEC is located at each longitude by using the northern edge of the SAC as its southern edge. Determining the northern edge of the current is more complicated. When locating it, the double-gyre structure of the subtropical gyre is ignored (Fig. 2). This decision was made because (1) the smaller-scale recirculation pathways are strongly influenced by mesoscale structures that cannot be fully resolved by the monthly fields derived herein; and (2) earlier studies define the SSEC in the upper layers as the flow from the Cape Basin diagonally across the South Atlantic to about 10–15°S at the western boundary (e.g. Stramma and Schott, 1999). Wherever possible, the northern edge of the current is identified as the latitude where the sign of the transport changes. If the transport does not change the direction at any latitude north of the southern edge, then the northern edge of the current is defined as the latitude where the transport is smallest. Once the boundaries of the current have been determined the transport is derived for each month in all years. The resulting latitudinal boundaries and zonal transports are used to estimate their climatological means and standard deviations. The left panels in Fig. 4 show the zonal transports while the right panels show the meridional boundaries of the SSEC for each layer. Below 800 m, the transport estimates east of the Greenwich Meridian are less

<sup>3</sup> The transports from the full time series (not shown) range from 8.5 Sv to 21.8 Sv. Deriving the time means at each grid point results in transports ranging from 11.4 Sv to 19.4 Sv.

<sup>4</sup> The transports from the full time series (not shown) range from 0.0 Sv to 9.2 Sv and the longitude dependent range of the time means is 0.4 Sv to 3.8 Sv.

<sup>5</sup> In Schmid and Garzoli (2009) the location of the southern boundary was defined based on the structure of the zonal velocity rather than the location of the Subtropical Front. At the widest point the difference in the width of the SAC from these two definitions amounts to about 40% of the width estimated herein.

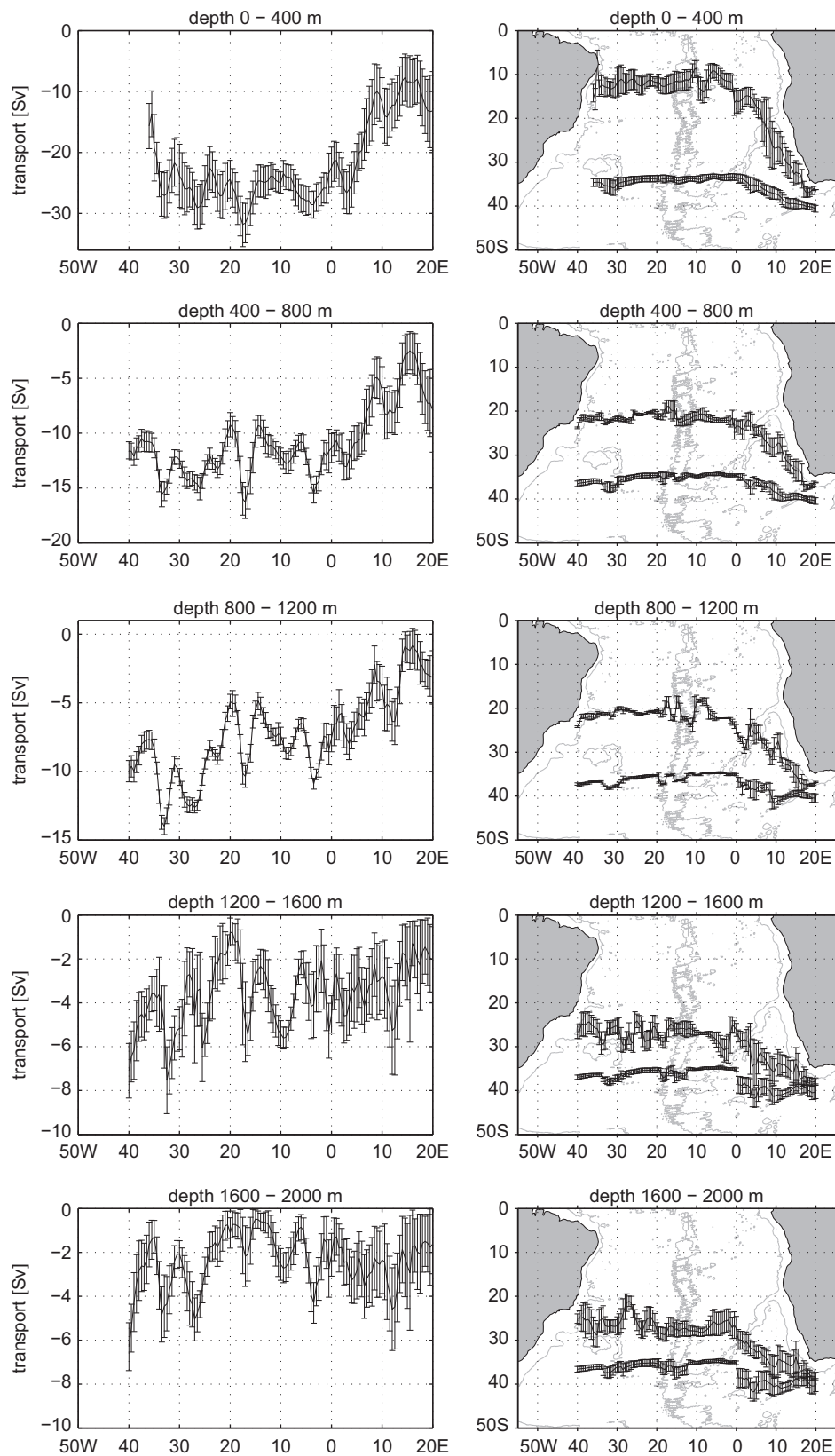


**Fig. 4.** Climatological zonal transport as a function of longitude (left) and maps depicting latitude limits (right) for the Southern South Equatorial Current as derived from the monthly estimates from all years. Error bars indicate the standard deviation. The right panels show the 3500 m isobath.

robust, because it is more difficult to determine the northern and southern boundaries of this current.

Similar to what was found for the SAC, the left panels in Fig. 4 reveal a longitude-dependence of the transports of the SSEC in all

400 m thick layers between the surface and 2000 m. In the 0–400 m layer the transports near the western boundary and especially near the eastern boundary are lower than in the interior (i.e., between 30°W and 5°E). In the west, the width of the current

is not changing and therefore the decrease is due to a reduction of the velocity. In the east the change of the transport is largely due to the change of the width of the current. It has to be noted that the absence of a significant longitude-dependence of the transport and the width of the current in the interior is different from the results obtained for the SAC.

The characteristics of the SSEC in the 0–400 m layer are mirrored in a large correlation (0.90) between the transport and the width of the current (0.12 higher than the correlation derived for the SAC in the same layer). With increasing depth, the correlation for the SSEC decreases quite rapidly by about 0.1 or more, which can be easily understood when looking at the transports and boundaries of the current in Fig. 4. In the 400–800 m layer the changes of the mean transport in the east are similar to those in the uppermost layer, but they are more noisy. This noisiness cannot be explained by the longitude-dependence of the width of the current. In addition, the drop-off of the transport near the western boundary in the 400–800 m layer occurs farther east than in the 0–400 m layer. The tendency towards noisy mean transports is also observed in the deeper layers. In addition, as mentioned above, the transport estimates near the eastern boundary, where the dependence of the transport on the width of the current is largest, are less robust than elsewhere. These two effects together cause the lower correlations in the deepest three layers. This strong depth-dependence of the correlation is different from the results for the SAC. An interpretation of the transport changes follows in Section 4.4.

As for the SAC (see Section 4.1), the longitude-dependence of the transport of the SSEC in the 800–1200 m layer can be compared with earlier results of Schmid and Garzoli (2009) for the 800–1100 dbar layer. Schmid and Garzoli (2009) found that the transport of the SSEC is about 6.3 Sv at 40°W and 1.8 Sv at 10°E (the corresponding standard deviations do not exceed 0.9 Sv). When adjusting their estimate to be representative for a 400 m thick layer as well as differences in the width of the current at 40°W (33%), then the transport difference between the two longitudes is about 8.0 Sv in the earlier study. For comparison, the overall means for the 800–1200 m layer are 9.5 Sv within 2° of 40°W and 4.4 Sv within 2° of 10°E, with standard deviations of 0.9 Sv and 1.9 Sv, respectively. The range of time means in the two longitude ranges is 8.8–10.0 Sv (around 40°W) and 2.2–6.4 Sv (around 10°E). Based on these numbers, the change of transports between 40°W and 10°E is 5.1 Sv with an uncertainty of about 2 Sv. As before, in the light of the statistical characteristics and the method-based differences of the two independent estimates of the transport, the new and the earlier result can be seen as consistent with each other. An interpretation of the longitude-dependence of this current follows in Section 4.4.

#### 4.3. Meridional transports in the subtropical gyre

The longitude-dependencies in the interior are consistent with pathways within the subtropical gyre that carry water northward from the SAC to the SSEC as suggested in earlier studies (e.g. Schmid et al., 2003; Schmid and Garzoli, 2009). The main interior pathway between the Greenwich Meridian and 20°W can be seen clearly in Figs. 2 and 5. The cumulative meridional transports at 35°S in Fig. 5 reveal five distinctive regimes in all five layers: (1) the eastern boundary regime dominated by the northward Benguela Current in the upper three layers (i.e., east of about 10°E); (2) the western boundary regime governed by the southward Brazil Current (i.e., west of about 50°W); (3) a regime with large-amplitude changes of the transport between 40°W and the Brazil Current; (4) an interior regime between 40 and 18°W with small amplitude changes of the transport; and (5) an interior

regime between 18°W and 1°E with a large northward transport in all layers.

With respect to the boundary currents it has to be cautioned that the shallow part of these currents next to the shelf break, at depths of less than 1000 m, and potentially also on the shelf cannot be captured with the method applied herein. However, these transports are typically small. Based on studies showing velocity or transport sections for the Brazil Current the underestimation of its transport is 1 Sv or less (e.g. Evans et al., 1983; Gordon and Greengrove, 1986). For the Benguela Current the underestimation due to limitations of the method adjacent to the shelf is expected to be even smaller. In support of this, for example, results of Stramma and Peterson (1989) and Garzoli and Gordon (1996) indicate that the current is typically found off-shore of the 1000 m isobath. Each of these regimes will be addressed in the following. Then the meridional transports will be analyzed in conjunction with the zonal transports of the SAC and the SSEC in Section 4.4.

##### 4.3.1. The eastern boundary regime

In the upper three 400 m thick layers the large northward transport at the eastern boundary at 35°S is associated with the Benguela Current (Fig. 5). The transports in these three layers are 13.4 Sv, 7.2 Sv and 3.3 Sv, respectively. Based on these numbers, the total transport of the Benguela Current in the upper 1200 m is 23.9 Sv. To investigate the latitude-dependence of the transports Fig. 6 shows estimates of the northward transport between the Greenwich Meridian and the eastern boundary, in a longitude range that was chosen by Garzoli et al. (2012) as the integration boundaries for the Benguela Current. They are used herein to allow a comparison of the independently obtained transports even though they lead to the inclusion of the small southward transports west of the Benguela Current (between 10°E and 1°E, Fig. 5), which leads to a small underestimation of the transport of this current. Nevertheless, these integration boundaries approximate the region dominated by this current quite well.

In 0–800 m and in 0–1200 m the transport increases by more than 10 Sv from 37°S to 32°S (black lines in Fig. 6). Most transports in the upper 800 m from Garzoli et al. (2012) agree quite well with the new results (gray dots in Fig. 6a). Even though direct comparisons are not straightforward due to different integration boundaries used in other previous studies (e.g. Stramma and Peterson, 1989; Gordon et al., 1992), one can still determine that the new results are consistent with their estimates which ranged from 25 Sv to 29 Sv in the latitude range of 28–32°S for a western integration limit within 5° of the Greenwich Meridian and a vertical integration limit within 300 m of the 1200 m shown in Fig. 6b. The deviation of up to 5 Sv can be seen as insignificant because it is within the uncertainties given by the standard deviations if enough estimates from the earlier study are available to get a robust mean. A larger difference between the transports can be seen at 34.5°S where the estimate of Garzoli et al. (2012) is based on a single section. It is noted that the transports from Garzoli et al. (2012) do not fully reveal the latitude-dependence found in the new results. This is most likely due to the much more limited number of transport estimates available in their study.

To the east of the Benguela Current a small poleward flow can be seen in the 400–800 m layer (–0.5 Sv) and the 800–1200 m layer (–1.3 Sv, Fig. 5). In the 1200–1600 m layer and the 1600–2000 m layer, a relatively strong southward transport (–2.1 Sv and –2.9 Sv, respectively) exists along the eastern boundary followed by a weak northward transport (0.8 Sv and 0.4 Sv, respectively), that is too deep to be part of the Benguela Current, to the west of it. To investigate the regional context of the southward transports at intermediate depths, Fig. 7 shows the

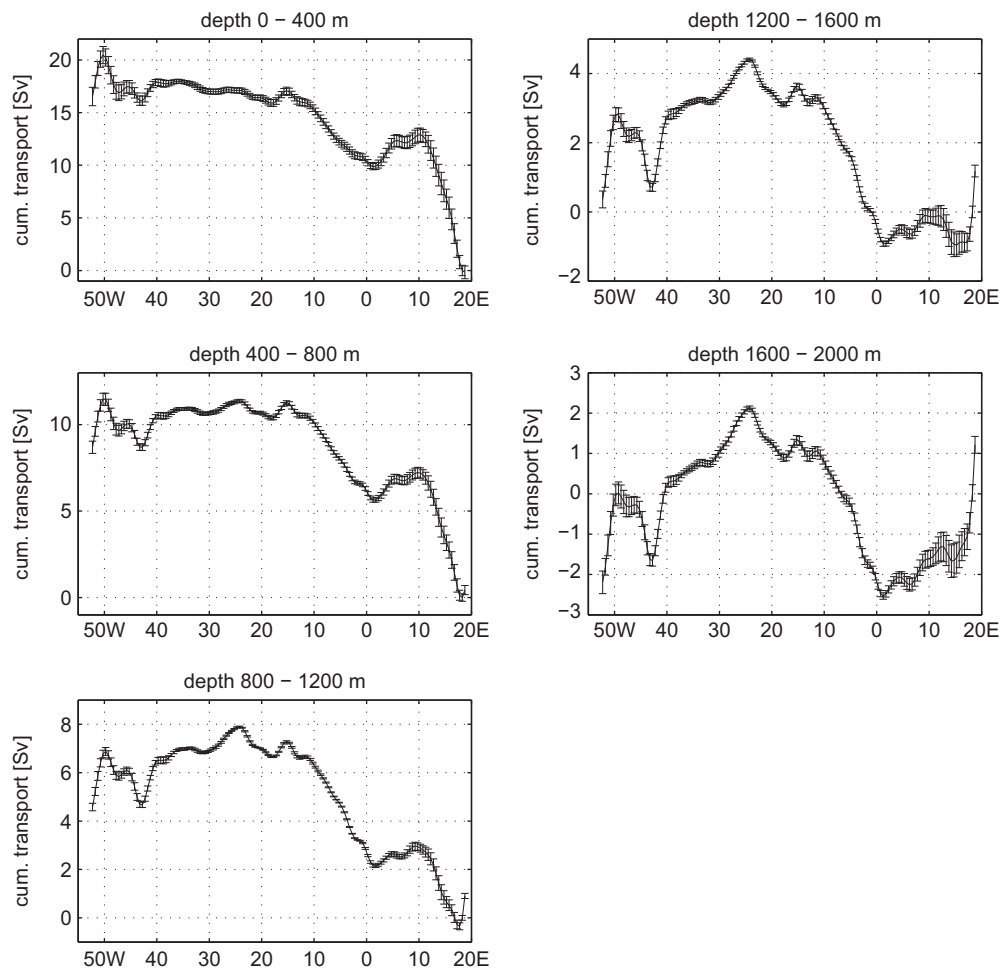


Fig. 5. Climatological cumulative meridional transport at 35°S as derived from the transports shown in Fig. 2. Error bars indicate the standard deviation.

salinity, pressure and circulation at the depth of the AAIW, which is characterized by a subsurface salinity minimum in its core. The pressure map reveals that the salinity minimum is mostly below 750 dbar, with the exception of an up to 7° wide band that extends from 24°S at 5°E to 35°S at the eastern boundary. The salinity map shows a southward spreading of high-salinity water along the eastern boundary all the way to 30°S and potentially even to 33.5°S, where a patch with elevated salinity can be seen. In general agreement with this, the velocity field reveals three areas with southward flow that indicate a southward spreading of the water along or close to the eastern boundary to 33.5°S. Because of the relatively poor data coverage in this region (Fig. 1), which increases the uncertainty of the velocity due to the pronounced mesoscale variability, it is of no big concern that there is no continuous southward flow in this region.

Many studies already reported that a poleward undercurrent is present under the Benguela Current (e.g. Chapman and Shannon, 1985; Duncombe Rae, 2005; Lass and Mohrholz, 2008; Veitch et al., 2010). This current was called the Benguela Poleward Undercurrent. Based on water properties this current can be seen as consisting of two parts (e.g. Duncombe Rae, 2005; Shillington et al., 2006). The upper part transports Central Water southward within the thermocline while the deeper part carries a relatively salty blend of AAIW towards the south. At the depth of the Central Water shown in Fig. 2e the poleward flow ends near 27°S, which is in agreement with Lass and Mohrholz (2008) as well as the workshop report “Benguela Current Large Marine Ecosystem

Programme (2007)”. Maps of the adjusted steric height generated by Reid (1994) also do not show southward flow extending farther south at or above 1000 dbar. In contrast to this, Richardson and Garzoli (2003) reported that some floats moved southward near the African continent at intermediate depths before being caught in the Benguela Current near the tip of South Africa. The results presented in Fig. 7 and discussed above indicate that such a pathway is possible but may not be very stable. The latter could explain the absence of such a flow in the map for 1000 dbar presented by Reid (1994). Similar to the new results, a modeling study of Veitch et al. (2010) showed that alongshore poleward flow, which deepens on the way to the south and is below about 600 m, extends into the southern Benguela Regime around 32°S (their Fig. 14), which agrees quite well with the southward extent found herein. Further research is needed to resolve how far south the Benguela Poleward Undercurrent extends, how the depth of this current depends on the latitude and how much it varies. Such an analysis is beyond the scope of this study.

#### 4.3.2. The western boundary regime

At 35°S the meridional transports at the western boundary decrease with increasing depth from 5 Sv in the 0–400 m layer to 2 Sv in the 1600–2000 m layer (Fig. 5). When expanding the analysis to other latitudes it is found that similar decreases of the alongshore transport are typical south of 35°S (Fig. 8). North of 35°S, the decrease with increasing depth typically ends in the

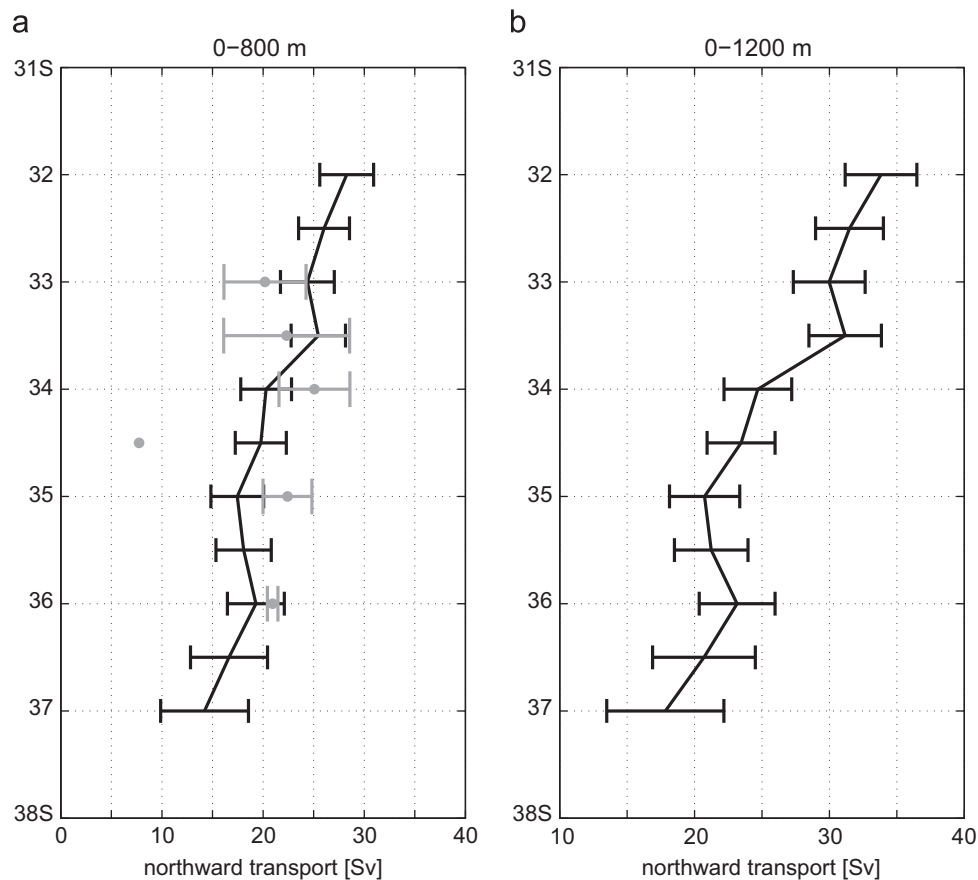


**Fig. 6.** Climatological mean northward transports between Greenwich and the eastern boundary in the upper 800 m (a) and in the upper 1200 m (b) as a function of latitude derived from the monthly means for all years are shown in black. Gray dots are based on transport estimates of Garzoli et al. (2012), which have error bars if more than one estimate exists within  $0.25^\circ$  of the latitude with the dot. All error bars indicate the standard deviation associated with the mean.

800–1200 m layer, and it is often followed by an increase in the deeper layers that can exceed 1 Sv from layer to layer. An example for this are the transport differences between the 1200–1600 m layer and the 1600–2000 m layer at and north of  $26^\circ\text{S}$ . This strengthening of the flow can also be seen in the maps of the transports for these two layers (Fig. 2g and h). In addition to the depth-dependence, Fig. 8 reveals that the transport in each layer increases from a minimum of less than 5 Sv at  $25^\circ\text{S}$  to a relative maximum in the range of 7–11 Sv at  $33^\circ\text{S}$  that is followed by a relative minimum of 2–7 Sv at  $36^\circ\text{S}$  and another maximum of 5–13 Sv at  $39^\circ\text{S}$ . In addition, there is a relatively weak minimum near  $32^\circ\text{S}$ . The overall increase of the southward transport between  $25^\circ\text{S}$  and  $31.5^\circ\text{S}$  can be understood quite easily when looking at the maps of the transport (Fig. 2), which show westward flow throughout this latitude range. Farther south, the relatively sharp increase in the 0–400 m layer between  $32^\circ\text{S}$  and  $33^\circ\text{S}$  is associated with water from the recirculation of the Brazil Current that feeds into the boundary current (Fig. 2b–d, more information on this recirculation follows in Section 4.3.3). In the deeper layers the increase in this latitude range is partly due to a recirculation and partly due to westward flow reaching the boundary (Fig. 2e–h).

In the following, the focus will be on the transports in two layers (Fig. 9). The 0–800 m layer represents the Brazil Current, while the 0–2000 m layer includes the recirculating Antarctic Intermediate Water and Upper Circumpolar Deep Water. The benefit of these two layers is that the transports derived herein can be compared with earlier estimates. Transports for the upper 800 m from a study of Garzoli et al. (2012) at latitudes where they

had data from multiple transects ( $24.5\text{--}25^\circ\text{S}$  and  $34.5\text{--}35.5^\circ\text{S}$ , indicated by gray dots with error bars in Fig. 9a) are tendentially higher than the transports derived herein, but that difference is within the uncertainty of the estimates as indicated by the standard deviation. The same is the case for the relatively low transport at  $33^\circ\text{S}$ , indicated by a gray triangle with error bar in Fig. 9a, that is based on two estimates of Stramma (1989). The relatively large difference between the new and the earlier transports from two transects at  $32^\circ\text{S}$ , depicted by the gray triangle from Stramma (1989) and the gray dot from Garzoli et al. (2012), are not of a big concern, because of the wide range of transports that gave rise to the large standard deviations of the other earlier estimates. Another study, by Rodrigues et al. (2010), estimated transports of 20.9 Sv at  $30^\circ\text{S}$  and 46.0 Sv at  $35^\circ\text{S}$  for a layer extending from the surface to 1000 dbar. The former is about twice as large as the new estimate of about 10 Sv in the upper 1000 m, while the latter is about three times larger than the new estimate of about 16 Sv in the upper 1000 m as well as significantly larger than most earlier results in both the 0–800 m and 0–2000 m layers (Fig. 9). It seems very likely that the transports derived by Rodrigues et al. (2010) are so large because they are based on an insufficient amount of data to determine the mean. For example, their large transport at  $35^\circ\text{S}$  is dominated by the barotropic component of their flow field, which shows a small strong anticyclonic recirculation of about 28.5 Sv to the east of the Brazil Current that is most likely caused by the lack of sufficient Lagrangian data to determine the mean barotropic flow in that region.

Proceeding to the layer from the surface to 2000 m one can also see a generally good agreement between the new and the earlier

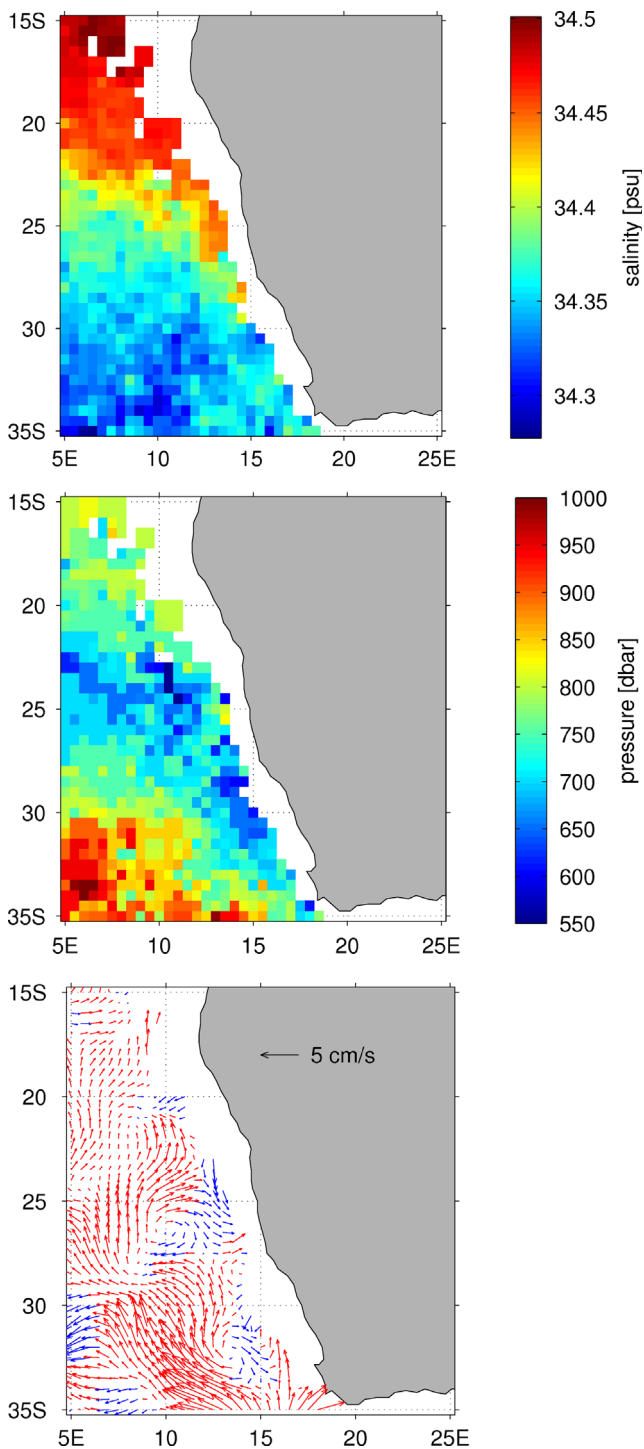


**Fig. 7.** Maps of climatological salinity, pressure and velocity at the salinity minimum of the Antarctic Intermediate Water. Colors of the vectors in the lower panel are the same as in Fig. 2. (For interpretation of the references to color in this figure caption in black-and-white copies, the reader is referred to the web version of this paper.)

transports, both for most estimates of Garzoli et al. (2012, gray dots) and the estimate of Zemba (1991, gray circle) at 34°S (Fig. 9b). One earlier estimate at 34°S of Garzoli et al. (2012) deviates quite strongly from the new results, which again is of no big concern because it is based on a single transect. Another estimate of Zemba (1991) with 69.9 Sv at 36°S is so large that it was not included in Fig. 9b. Potentially, this large transport is due to a strong deep-reaching eddy just east of the Brazil Current. Signs for such an eddy can be seen in the velocity section

presented by Zemba (1991). Overall, the generally good agreement between the independent estimates of the transport (Fig. 9) increase the confidence that the latitude-dependence visible in Figs. 8 and 9 is realistic. The characteristics of this pattern will be described in the following.

The transports of the Brazil Current shown in Fig. 9a reveal three minima, with 3.1 Sv, 12.6 Sv and 11.4 Sv at 27°S, 32°S and 36°S, respectively. The maxima are 15.3 Sv at 31.5°S, 20.7 Sv at 33°S and 22.2 Sv at 39°S. As was already apparent from Fig. 8, the latitude-dependence of the total transport in the upper 2000 m follows a similar pattern to that in the upper 800 m, i.e., most maxima and minima are found at the same latitudes as in the upper 800 m (Fig. 9). After an overall decrease of about 6 Sv between 25 and 27.5°S, the transport increases gradually with latitude from a minimum of 5.2 Sv at 28°S to a relative maximum of 33.3 Sv at 31.5°S. It then decreases again to 29.0 Sv at 32°S before increasing to 44.2 Sv at 33°S. Continuing southward the transport drops once again to 22.2 Sv at 36°S before increasing to 38.7 Sv at 39°S. As discussed in the first paragraph of this section, the increase in the northern half of the shown latitude range can be attributed to the westward flow reaching the boundary, while the smaller but relatively sharp increase between 32°S and 33°S can be attributed partly to the recirculation of the Brazil Current (see next section) for the 0–800 m layer and to the westward flow in the SSEC in the 400–800 m layer.

#### 4.3.3. The large-amplitude regime between 40°W and the Brazil Current

The northward flow immediately east of the Brazil Current in Fig. 5 is part of a recirculation cell of the Brazil Current (e.g. Gordon and Greengrove, 1986; Stramma, 1989). At 35°S the northward transports in this cell are 4.3 Sv, 2.8 Sv, 2.2 Sv, 2.1 Sv and 1.7 Sv in the five layers. These numbers add up to a total transport of 13.1 Sv, which is in very good agreement with the estimate of 13.2 Sv at 34°S that Zemba (1991) derived for a layer extending from the surface down to the lower boundary of the Upper Circumpolar Water (which is close to 2000 m). Also, Stramma (1989) estimated a transport of 7.5 Sv in the upper 800 m south of 28°S for this recirculation, which again agrees well with the new estimate of 7.1 Sv (as derived from the transports in the upper 2 layers at 35°S). Based on the Brazil Current transports derived herein, the northward transport in this recirculation cell feeds back into the Brazil Current north of 33°S, and the estimates for both layers are in very good agreement with the change of the alongshore transport between 32°S and 33°S (Fig. 9). For the upper 800 m this change is 8.1 Sv (to be compared with the 7.1 Sv), while it is 15.2 Sv (to be compared with the 13.1 Sv) in the upper 2000 m. The standard deviations for all four transports going into the calculation of the changes of the Brazil Current transports are about 3 Sv and therefore the imbalances of less than about 2 Sv are insignificant.

Farther offshore, around 43°W, two bands of opposing flow with meridional transports on the order of 2 Sv can be seen in all layers. The cause for this could be a southward excursion of the SSEC as indicated by the southward dip of the contour lines depicting the latitude where the zonal velocity goes to zero in Fig. 2.

#### 4.3.4. The interior regime between 18°W and 1°E

A large change of the cumulative meridional transport between 18°W and 1°E is present in all five of the 400 m thick layers (Fig. 5). The transport in this region of interior northward flow shrinks with increasing depth from 6.8 Sv in the uppermost layer to 3.9 Sv in the deepest layer. In the three layers in between 400 m and 1600 m the transports are 5.6 Sv, 5.1 Sv and 4.6 Sv, respectively.

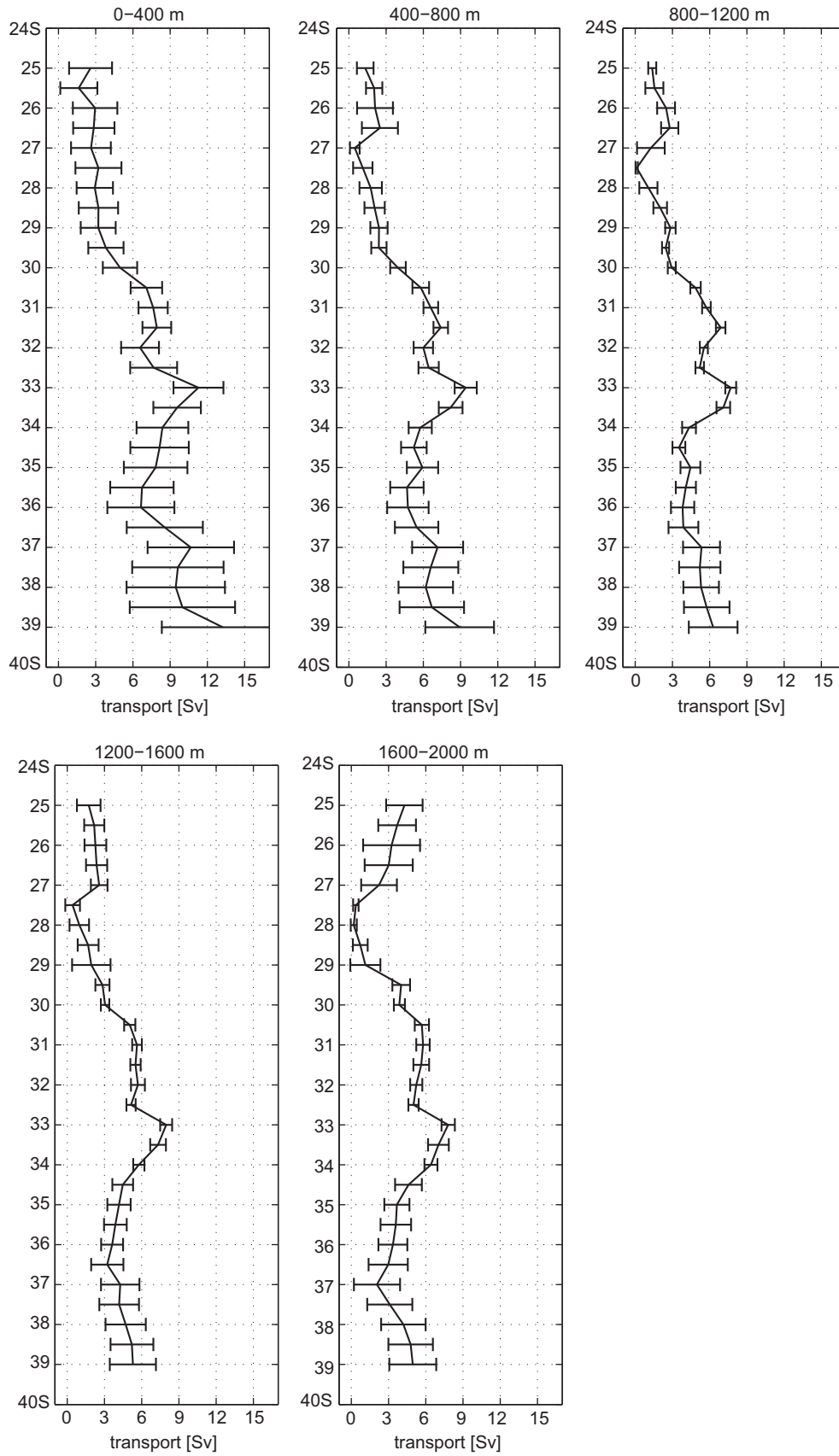


**Fig. 8.** Climatological mean transports along the western boundary in five layers as a function of latitude derived from the monthly means for all years. Error bars indicate the standard deviation.

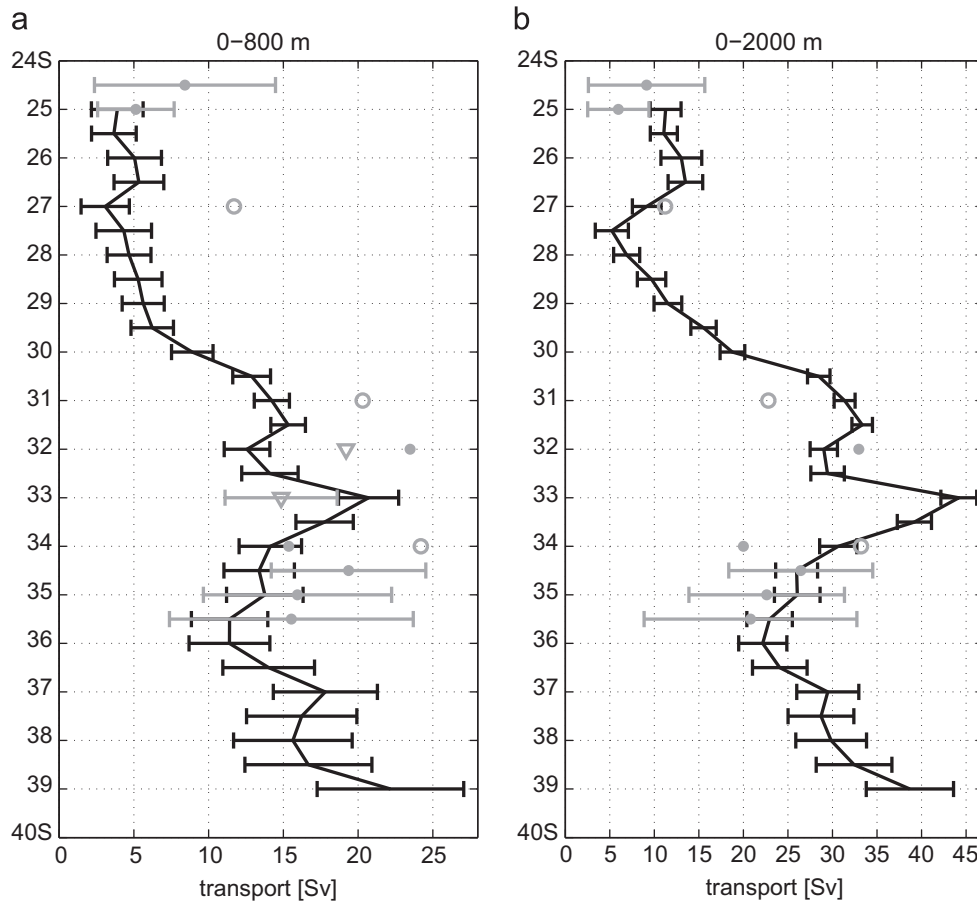


**Fig. 9.** Climatological mean transports of the Brazil Current (a) and in the upper 2000 m (b) as a function of latitude derived from the monthly means for all years are shown in black. Gray triangles depict transport estimates of Stramma (1989), the gray circle shows a transport estimate of Zemba (1991), and the gray dots are based on transport estimates of Garzoli et al. (2012). The latter also have error bars if more than one estimate exists within  $0.25^\circ$  of the latitude with the dot. All error bars indicate the standard deviation associated with the mean. The transports in the five layers that were used for the shown estimates are presented in Fig. 8.

The sum of the transports in the five layers yields a total northward transport of 26.0 Sv for the upper 2000 m. Earlier studies also found northward flow in this region (e.g. Reid, 1989; Stramma and England, 1999; Schmid and Garzoli, 2009), but they provided less details on the horizontal and vertical structure of the flow because of a much smaller availability of observations. A study by Schmid et al. (2000) showed that these northward transports can be explained on the basis of the Sverdrup dynamics.

#### 4.3.5. The interior regime between $40^\circ\text{W}$ and $18^\circ\text{W}$

West of the interior region with large northward transports, the transport alternates between southward and northward, with two bands of northward and two bands of southward transport between  $18^\circ\text{W}$  and  $40^\circ\text{W}$  (Fig. 5). The two bands of northward transport are about  $6^\circ$  wide and have a transport of about 1 Sv in all five layers. In the uppermost layer, the northward transports dominate, i.e., the largest cumulative transport is found at  $40^\circ\text{W}$ . This is not the case in the other layers. In the 400–800 m layer, the northward and southward transports are almost the same (the cumulative transports at  $18^\circ\text{W}$  and  $40^\circ\text{W}$  are within 0.1 Sv of each other), while the southward transports dominate in the deeper layers. These differences between the layers are due to the size of the southward transports. In the shallowest layer, the southward transports in the bands around  $28^\circ\text{W}$  and  $37^\circ\text{W}$  are smaller than 0.3 Sv. In the 400–800 m layer the southward transports in these bands are 0.4 Sv and 0.7 Sv, respectively. Going deeper, one finds similar or larger southward transports in these two bands (up to

about 1.4 Sv near  $28^\circ\text{W}$ ). Similar to the situation farther west, which is described in Section 4.3.3, this could be associated with the southward excursions of the SSEC as indicated by the southward dip of the contour lines depicting the latitude where the zonal velocity goes to zero (Fig. 2f and g).

#### 4.4. Joint analysis of the zonal and meridional transports in the subtropical gyre

In earlier studies, the changes of the SAC between  $30^\circ\text{W}$  and the Greenwich Meridian were discussed (e.g. Stramma and Peterson, 1990; Peterson and Stramma, 1991; Smythe-Wright et al., 1998; Rodrigues et al., 2010). The four main scenarios addressed in these studies are: (1) the Mid-Atlantic Ridge causes a reduction of the SAC transport (e.g. Stramma and Peterson, 1990; Peterson and Stramma, 1991); (2) part of the water in the SAC recirculates in the interior of the subtropical gyre throughout a large part of the basin (e.g. Peterson and Stramma, 1991); (3) part of the water in the SAC recirculates in the interior of the subtropical gyre west of  $20^\circ\text{W}$  (e.g. Smythe-Wright et al., 1998); and (4) the SAC splits up into a southern (south of  $41^\circ\text{S}$ ) and a northern (north of  $38^\circ\text{S}$ ) branch near  $7^\circ\text{W}$  (Rodrigues et al., 2010).

To address the underlying dynamic of the transport changes of the SAC and also the SSEC, Fig. 10 combines the zonal transports at longitudinal boundaries between the regimes described above as well as at additional longitudes with the meridional transports between these longitudes in five 400 m thick layers. No transport estimate for the SSEC is shown at  $40^\circ\text{W}$  in the shallowest layer,

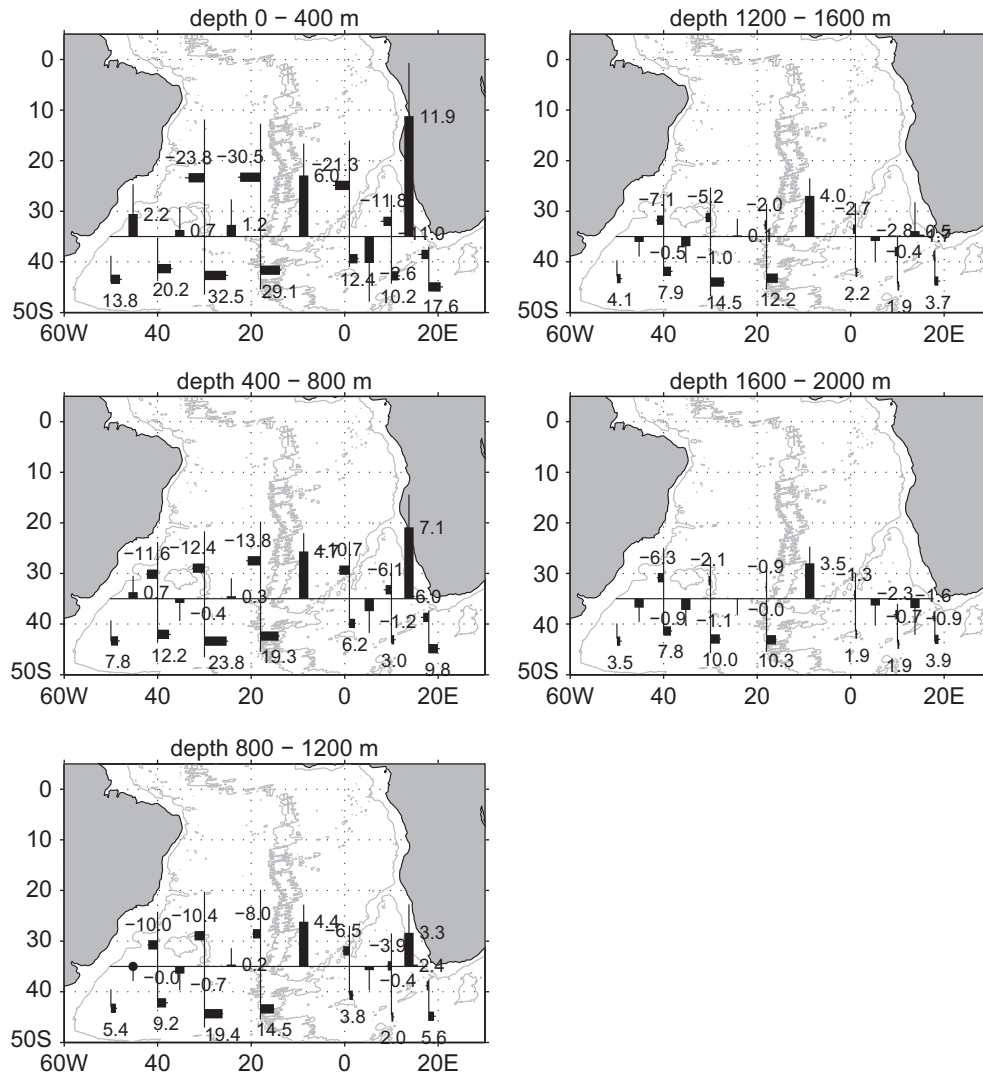


**Fig. 10.** Gyre transports at selected longitudes and latitudes derived from the monthly estimates from all years. Error bars indicate the standard deviation. Meridional transports are for 35°S. For the sake of visibility of the bars and error bars representing meridional transports different scales were used to represent meridional and zonal transports. All panels show the 3500 m isobath.

because this longitude is too far west to allow for defining the northern boundary of this current.

Before interpreting the relationships between zonal and meridional transports the sources of uncertainties of the zonal transports need to be identified. For the SAC the uncertainties are largest in the Brazil–Malvinas Confluence in the west and in the eastern Cape Basin (near South Africa). Both regions are dominated by large mesoscale variability which gives rise to, for example, the larger standard deviations near the western boundary in the top right panel of Fig. 3 and in the vicinity of the eastern boundary in the lower two panels of Fig. 3. Away from the boundaries, the mesoscale variability is smaller, but the complication for estimating the transport of the SAC is nevertheless related to the uncertainty associated with separating this current from the ACC by determining where the transport minimum nearest to the Subtropical Front is (Section 4.1). It has to be kept in mind that changes of the transport of the SAC in the interior that cannot be explained by meridional transports from the SAC to the SSEC may be due to cross-frontal transports between the SAC and the ACC as well as uncertainties about where exactly the boundary between the two currents is. For the SSEC the reason for large uncertainties is the difficulty in determining the northern boundary of this current,

especially near the western boundary in the shallowest layer. Also, the zonal transports near the eastern boundary do not fully reflect the transport of the SSEC due to the meridional component of its flow.

Between 1°E and 18°W, in the interior longitude range with the largest northward transport, the zonal transport of the SAC decreases in all layers and these changes of the zonal transports are consistent with the northward transport within the uncertainty of the estimates. While the drop-off of the zonal transport in the SAC starts at the western edge of the Mid-Atlantic Ridge when defined as the western longitude where the water depth is 3500 m, it does not end when the water depth increases again on the eastern side of the ridge (Fig. 3). This characteristic excludes scenario 1 (the Mid-Atlantic Ridge) as the cause for the drop-off of the zonal transport of the SAC and supports scenario 2 (recirculation in the interior in a large part of the basin). The narrowing of the SAC that mainly occurs in the Cape Basin does leave some room for scenario 4 (that the SAC splits up), however, because of the high mesoscale variability in this region it is not yet clear what exactly is happening to the SAC. Potentially, some of its water is entrained into the ACC here.

With respect to the SSEC the meridional transport between 1°E and 18°W agrees well with the changes of the zonal transport in

the upper three layers. When going deeper, in the deepest two layers, there is a relatively large imbalance of the transports for the SSEC. This is most likely an artifact of a large uncertainty of the width of the current and the estimated zonal transports (Fig. 4). Therefore, more observations are needed to get robust estimates of the mean zonal flow below 1200 m in this region.

West of 18°W the transport of the SAC tends to increase from west to east in all layers until it reaches a relative maximum near 30°W in most layers (Fig. 3). This longitude-dependence does not support scenario 3 (recirculation west of 20°W as an explanation for the decrease of the SAC transport between 30°W and the Greenwich Meridian) and it cannot be explained by meridional transports from the north into the SAC because many of these transports are, on average, northward and those that are southward are too small (Fig. 10). The most likely explanation for this longitude-dependence is that the Zapiola Eddy causes a split of the zonal flow, with the larger part heading east to the south of it. Some of that water can join the SAC east of the Zapiola Eddy, while most of it stays south of the Subtropical Front and thus remains in the ACC. This possibility is supported by the predominance of northward flow to the east of the Zapiola Eddy (Fig. 2).

For the SSEC the transport west of 18°W decreases from east to west in the upper two layers. However, the decrease in the shallowest layer occurs primarily very close to the western boundary, while the decrease in the second layer is insignificant (Fig. 4). In the 800–1200 m layer the transport increases significantly from east to west before dropping off again. In the two layers below 1200 m the transport is very variable with only a slight increase. This increase in the deepest two layers is associated with a widening of the current that can be interpreted as horizontal entrainment of water from the north into the SSEC. This could be an explanation for the fact that there is no sign for a balance between the quite large changes of the zonal transports and the relatively small meridional transports to the south (instead of northward, Fig. 10). More observations are needed to clarify this issue.

## 5. Summary and conclusions

Data from Argo floats and sea surface height from altimetry are combined to derive a three-dimensional velocity field for the South Atlantic that extends from the surface down to 2000 dbar. The results of an analysis of this velocity field increase the understanding of the three-dimensional structure of the subtropical gyre in the South Atlantic (e.g. Boebel et al., 1999; Stramma and Schott, 1999; Rodrigues et al., 2007) as well as the longitude and depth-dependence of the transports in it (e.g. Schmid et al., 2000; Schmid and Garzoli, 2009).

With increasing depth, the latitudinal extent of the subtropical gyre becomes smaller by about 10° between the surface and the depth where the Antarctic Intermediate Water is found (see Fig. 2 and Section 3). Below that depth the gyre shrinks by another 5°. Most of this change is due to a southward shift of the westward flowing branch of the subtropical gyre with increasing depth that is most pronounced near the western boundary. This pattern is consistent with the Sverdrup dynamic that governs subtropical gyres (e.g. Schmid et al., 2000).

The new results also reveal a small area within the subtropical gyre near the western boundary where the zonal flow is reversed (see Fig. 2b and Section 3.1). This reversal can be associated with the double-celled subtropical gyre that has been found in estimates based on observations of the sea level by Vianna and Menezes (2011). In an expansion of their earlier work, the new velocity fields reveal a reduction of the size of this feature with increasing depth (see Fig. 2b and c, and Sections 3.1 and 3.2).

The zonal transports estimated for the South Atlantic Current (SAC) and the Southern South Equatorial Current (SSEC) reveal a pronounced longitude-dependence in most 400 m thick layers between the surface and 2000 m (see Figs. 3 and 4, and Sections 4.1 and 4.2). For example, a west to east decrease of the transport of the SAC between 18°W and 1°E of 15.0 Sv with an uncertainty of about 4 Sv has been derived for the 800–1200 m layer (Section 4.1). Similarly, the transport of the SSEC increases by 5.1 Sv between 10°E and 40°W in the same layer, with an uncertainty of about 2 Sv (Section 4.2). For both currents, a detailed comparison of these estimates with earlier results for the Antarctic Intermediate Water (AAIW) layer reveals good agreements, within the uncertainty of the estimates. The new velocity fields show that the longitude-dependence of the SAC transport has a very similar shape in all five layers. In contrast to this, the longitude-dependence of the SSEC transport changes significantly from layer to layer. In addition to providing more detailed information of these currents as a function of depth, the new velocity fields also allow a more detailed analysis of this longitude-dependence in conjunction with the meridional transports. This analysis will be summarized after taking a look at the meridional transports near the boundaries and in the interior.

Northward transports of the Benguela Current decrease quite strongly with increasing depth from 13.4 Sv in the upper 400 m at 35°S to 3.3 Sv in 800–1200 m at the same latitude, yielding a total transport of 23.9 Sv (see Figs. 5 and 6, and Section 4.3.1). Estimates of the transports at different latitudes reveal an increase by more than 10 Sv from 37°S to 32°S, both in the upper 800 m and the upper 1200 m. For the thinner layer, this latitude-dependence agrees quite well with results based on independent transport estimates at a smaller number of latitudes that do not cover the full latitude range considered herein.

Southward transports at the eastern boundary, east of the Benguela Current, at 35°S are found in the four 400 m thick layers between 400 m and 2000 m (see Figs. 5 and 7, and Section 4.3.1). The salinity minimum of the AAIW reveals relatively high salinity at 33.5°S that could originate from the north. In the 400–800 m and the 800–1200 m layers Fig. 5 shows southward flow that can be associated with the Benguela Poleward Undercurrent. This flow extends to 33.5°S in the deeper layer, which is farther south than suggested by the results of earlier studies. Lass and Mohrholz (2008) reported that this current extends to 27°S, while Veitch et al. (2010) found it at 32°S. More observations are needed to determine the meridional extent and the variability of this current.

Along the western boundary a strengthening of the Brazil Current (in 0–800 m) from 3.1 Sv at 27°S to 15.3 Sv at 31.5°S can be attributed to the westward transport of the SSEC (see Figs. 8 and 9, and Section 4.3.2). After a relatively small decrease in 31.5°S to 32°S the transport of the Brazil Current increases once again from 12.6 Sv at 32°S to 20.7 Sv at 33°S. The maps of the transports in Fig. 2 show that this increase is largely due to the recirculation of the Brazil Current, especially in the upper 400 m, and to a lesser extent to the portion of the SSEC that flows westward between these two latitudes. From 33°S to 36°S the transports weaken to 11.4 Sv before strengthening again to 22.2 Sv at 39°S. A similar pattern exists in the transports integrated over the upper 2000 m. These results can be considered to be robust, because comparisons with earlier transport estimates at a small number of latitudes, that do not allow a detailed analysis of their latitude-dependence, reveal mostly good agreements.

The small recirculation cell of the Brazil Current was found in all five 400 m thick layers, i.e. not just in the depth range governed by the Brazil Current but also at greater depths, with transports between 4.3 Sv in the 0–400 m layer and 1.7 Sv in the 1600–2000 m layer at 35°S (see Fig. 5 and Section 4.3.3). The transport of this recirculation is 7.1 Sv in the upper 800 m (the Brazil Current) and 13.1 Sv in the upper 2000 m, respectively. Both estimates

agree quite well with results from earlier studies and within the uncertainty of the estimates they are in agreement with the changes of the alongshore transport between 32°S and 33°S that amounts to 8.1 Sv for the upper 800 m and 15.2 Sv for the upper 2000 m.

An analysis of zonal and meridional transports in the subtropical gyre reveals an interior pathway from the SAC to the SSEC between 18°W and 1°E with transports between 6.8 Sv and 3.9 Sv in five 400 m thick layers from the surface to 2000 m (see Fig. 10, and Sections 4.3.4 and 4.4). The total northward transport in the upper 2000 m adds up to 26.0 Sv. Within the uncertainty of the estimated transports these northward transports are consistent with the changes of the zonal transports in the SAC and SSEC. This pathway is consistent with a scenario proposed by Peterson and Stramma (1991), that part of the transport in the SAC recirculates in the subtropical gyre throughout a large part of the basin between 30°W and the Greenwich Meridian, and it does not support a role of the Mid-Atlantic Ridge (e.g. Stramma and Peterson, 1990; Peterson and Stramma, 1991) or a recirculation west of 20°W (e.g. Smythe-Wright et al., 1998).

Farther west, between 40°W and 18°W the meridional transports are quite small and very variable (see Section 4.3.5). In this region, the balance between changes of the transports in the two zonal branches of the subtropical gyre and the meridional transports is quite poor (see Fig. 10 and Section 4.4) in most layers, especially for the SAC due to the presence of the Zapiola Eddy (see Fig. 2 and Section 3).

Plans for the future are to expand on this work with the goal to study seasonal to interannual variability of the circulation in the South Atlantic by taking advantage of the constantly increasing amount of Argo observations. This is expected to improve the ability to monitor the circulation in the South Atlantic.

## Acknowledgments

Thanks to everybody involved in the Argo project for their contributions to generating a high-quality global sub-surface data

set. Thanks also to Marlos Goes, Renellys Perez and Christopher Meinen for useful suggestions.

## Appendix A. Deriving fields of the dynamic height

The approach is to derive the dynamic height for each profile that has good salinity and temperature measurements (see Section 2 on the profile data used). These profiles are then used to obtain gridded fields of the mean dynamic height for each month of the period March 2000 to June 2012 on a 0.5° by 0.5° grid with a vertical resolution of 10 dbar. Similar to an approach used by Willis (2010), the individual profiles are used to generate synthetic profiles of the dynamic height on the same grid based on linear fits between them and the sea surface height from AVISO (see Section 2 on the altimetry data used). To achieve this all profiles and the corresponding sea surface heights within a 5° by 2° box around each grid point are assembled. If at least 10 data pairs are available for a given grid point, then the correlation between them is calculated and a linear fit is derived at each pressure level. The correlations are quite good throughout the study region (e.g. at 1000 dbar, Fig. 11a). A comparison of the annual climatologies of the two dynamic height fields at 1000 dbar from in situ observations (Fig. 11b) and from the empirical relationship between dynamic height and sea surface height (Fig. 11c) shows that they agree quite well.

## Appendix B. Estimating the relative geostrophic velocity

The zonal and meridional components of the relative geostrophic velocity are estimated from the gradients of in situ as well as the synthetic dynamic height fields with a level of no motion at 1000 dbar for each month in the period covered by this study. Merged velocity fields are then obtained by using the velocity from the synthetic dynamic height field at a grid point in a given month if no velocity could be derived from the in situ dynamic height field at that location. The geostrophic velocities at 20 dbar relative to a level of no motion at 1000 dbar from the merged fields for January 2011 illustrate the main characteristics of the

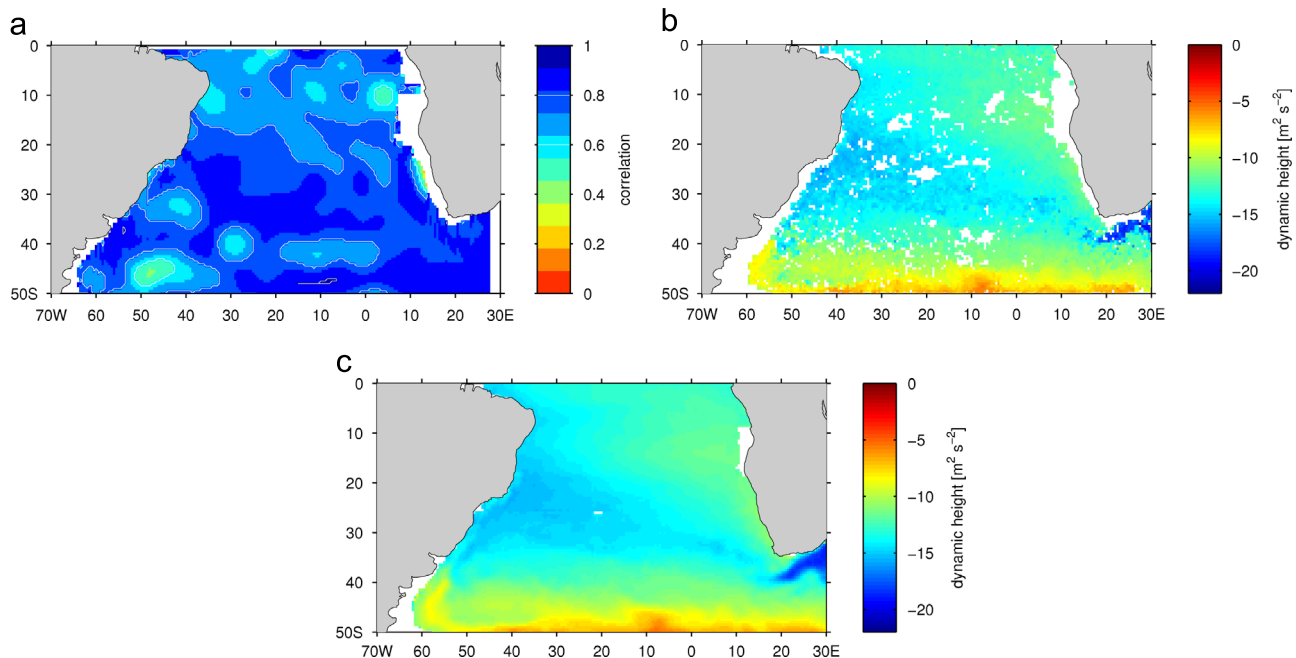


**Fig. 11.** (a) Correlation between sea surface height and dynamic height at 1000 dbar. (b) Climatology of the dynamic height at 1000 dbar from in situ observations. (c) Climatology of the dynamic height at 1000 dbar calculated using the fits quantifying the relationship between the sea surface height from AVISO and the in situ dynamic height. (For interpretation of the references to color in this figure caption in black-and-white copies, the reader is referred to the web version of this paper.)

large-scale circulation in the South Atlantic quite well (Fig. 12a and b), as will be discussed in Appendix C.

### Appendix C. Deriving the absolute geostrophic velocity

Trajectories from profiling floats and subsurface floats are used to determine the subsurface velocity needed for the barotropic adjustment of the relative geostrophic velocity, this has also been called the level of known motion approach. How this processing and the adjustment are done is described in the following.

Profiling floats pose a challenge when it comes to estimating their subsurface drift velocity. Two main factors are important in this context: (1) Profiling floats typically spend some time on the

surface during which their position has not been measured. (2) It takes profiling floats several hours to ascend from the drift depth to the surface and descend back to the drift depth. In most cases, the first factor has a larger impact on the estimation of the subsurface velocity than the second factor, because the velocity at the surface is larger than the velocity encountered during the ascent or descent. A more accurate surface drift of the profiling floats has been derived using an extrapolation method that is based on the approaches used by Schmid et al. (2001) and Davis et al. (1992) both of which used cokriging. The difference between their methods is the choice of the structure function that was used to derive fits to the dissimilarities (the variogram) estimated from the data. Schmid et al. (2001) used a structure function that only works in the tropics and described the approach in detail in their

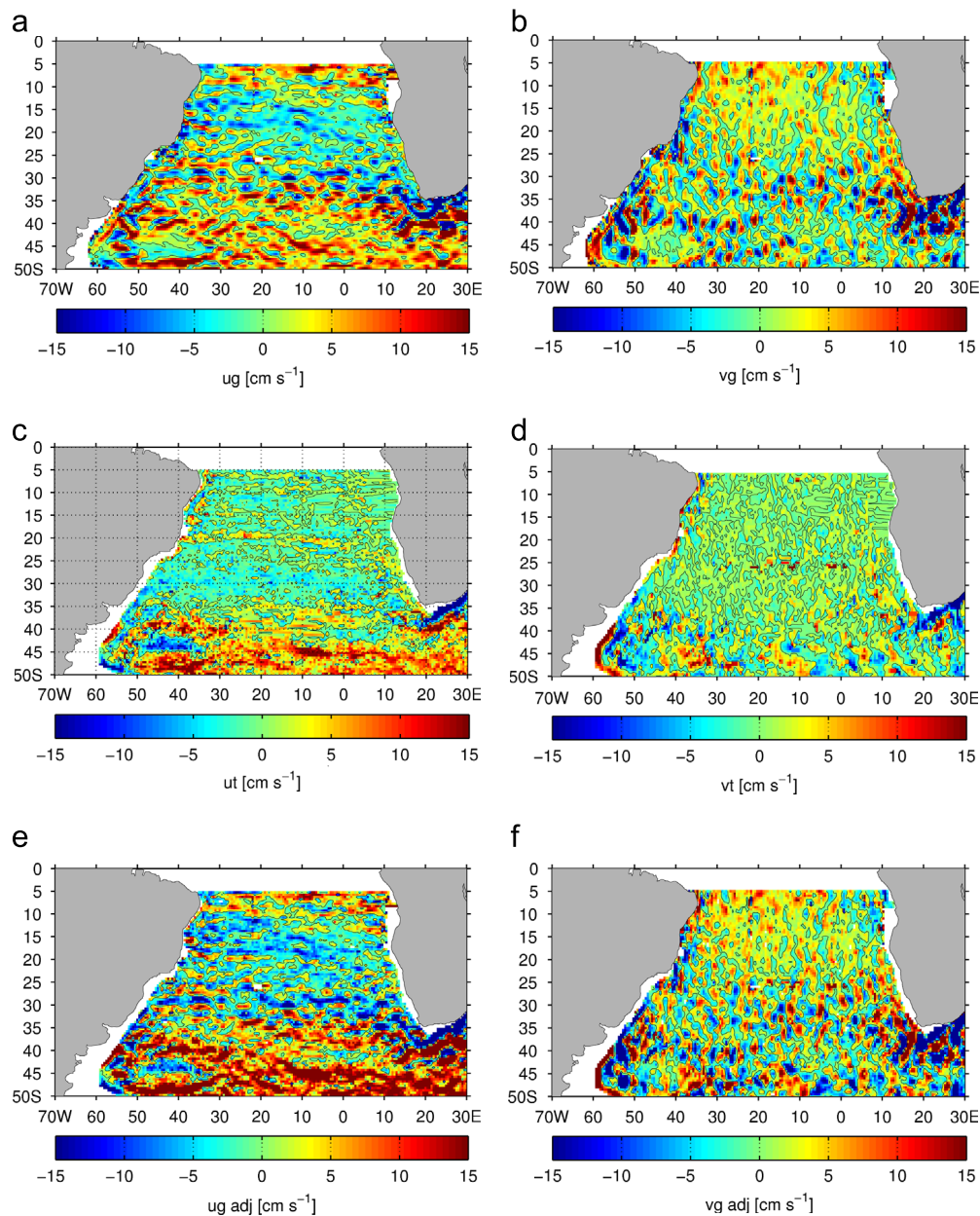


**Fig. 12.** Maps of the mean fields of the horizontal velocity for January 2011. Top: geostrophic velocities at 20 dbar, obtained with a level of no motion at 1000 dbar. The estimates are based on statistical mean and synthetic profiles of the dynamic height estimated using the correlation between and in situ observations. Middle: Mean fields of the absolute subsurface velocity from the float trajectories (climatological velocity estimates are used if needed, as described in the text). Bottom: geostrophic velocity at 20 dbar, adjusted with the absolute subsurface velocity. Left: zonal velocity. Right: meridional velocity. (For interpretation of the references to color in this figure caption in black-and-white copies, the reader is referred to the web version of this paper.)

**Table 1**

Fixed-value parameter sets used for the cokriging. Scale 1 is the velocity scale for the low-frequency variability. Scale 2 is the velocity scale for the high-frequency variability. Scale 3 is the time scale for the low-frequency variability.

Set	Scale 1 [cm s <sup>-1</sup> ]	Scale 2 [cm s <sup>-1</sup> ]	Scale 3 [days]
1	20	5	1.5
2	10	10	1.5
3	40	10	1.5
4	60	20	1.5

appendix, while Davis et al. (1992) used a structure function and a set of coefficients that work well in the higher latitudes.

Herein, most of the domain is not in the tropics, therefore it is necessary to apply the structure functions used by Davis et al. (1992). The difficulty is that the quality of the solution depends on the positions measured during the surface phase as well as on the coefficients used in the structure function. To get the best solution, the extrapolation was performed for six different sets of coefficients. Four of these sets have fixed coefficients (Table 1) to allow for dynamical differences. The coefficients for the remaining two sets are estimated from the drift information collected during the surface period of a profiling float. One of these two sets uses the positions while the other uses the velocities for the derivation of the coefficients for the structure function. Following Davis et al. (1992), the position errors of each satellite fix are assumed to be 1000 m for all six sets. For all six solutions, the median velocity of the measured surface drift is compared with the median of the extrapolated surface drift to identify the best match for each cycle. Once this has been accomplished, the best estimates for the subsurface displacements for each profiling float can be determined and the zonal and meridional displacement velocities can be estimated.

Before the box-averaging can be done it is necessary to normalize the velocities from most floats in such a way that they represent daily means of the velocity, because their original data contain velocities that are representative of different time periods. Box-averaged subsurface velocities and associated pressures are then derived on the same grid as the one used for the geostrophic velocity profiles for each month and year of the study period. As an example, the resulting subsurface velocities for January 2011 are shown in Fig. 12c and d. These two fields and the corresponding pressure field (not shown) are used in conjunction with the 3-dimensional fields of the relative geostrophic velocity to estimate the absolute geostrophic velocity. To overcome the challenge that there are grid points with a geostrophic velocity profile that do not have a subsurface velocity in a given month, the climatological mean of the subsurface velocity (and its pressure) is used for the adjustment in these cases. The resulting adjusted geostrophic velocity fields at the 20 dbar level for January 2011 are shown in Fig. 12e and f.

As expected, the absolute geostrophic velocity field is more realistic than the relative geostrophic velocity (compare top and bottom row of Fig. 12): The eastward flow in the South Atlantic Current and Antarctic Circumpolar Current region is significantly stronger than in the unadjusted velocities, due to strong barotropic flow associated with both currents. The same is the case for both velocity components in the Brazil/Malvinas Confluence region, for the Zapiola Eddy, and in the region dominated by the Agulhas Current and its retroflexion. In contrast to this, the westward flow in the Southern South Equatorial Current did not change much due to the adjustment, which is not surprising because this current is known to be less barotropic than the other currents mentioned above. The same is the case farther north.

## Appendix D. Filling in small gaps

Small gaps in the absolute velocity fields that are surrounded by observations are filled with objective mapping using the method developed by Hiller and Käse (1983). The correlation length scales for longitude and latitude were both set to 3°. The root mean square error of the velocity and its climatological estimates are set to 2 cm s<sup>-1</sup> and 10 cm s<sup>-1</sup>, respectively. Based on an analysis of the resulting fields, grid points where the root mean square error of the method exceeds 4.9 cm s<sup>-1</sup> are excluded from the analysis. The resulting fields are smoothed with a second order Butterworth filter that has a length scale of 2° to remove the mesoscale signal from the velocity fields because it masks the large-scale features of the circulation.

## Appendix E. Adding the Ekman velocity

The zonal ( $u$ ) and meridional ( $v$ ) components of the Ekman (1905) velocity are

$$u = Ve^{(z/D_E)} \cos(\pi/4 + \pi z/D_E) \quad (\text{E.1})$$

$$v = Ve^{(z/D_E)} \sin(\pi/4 + \pi z/D_E), \quad (\text{E.2})$$

with the surface velocity  $V$  and the Ekman depth  $D_E$  defined by

$$V = \sqrt{2\pi\tau/(D_E\rho|f|)} \quad (\text{E.3})$$

and

$$D_E = \pi\sqrt{2A_z/|f|}, \quad (\text{E.4})$$

respectively. In these equations  $\tau$  is the wind stress,  $\rho$  is the water density,  $f$  is the Coriolis parameter,  $A_z$  is the friction coefficient and  $z$  is the depth. Rio and Hernandez (2003) derived friction coefficients for the world oceans for two different seasons. For the South Atlantic they reported that the coefficients vary between about  $10 \times 10^{-3} \text{ m}^2 \text{ s}^{-1}$  and about  $20 \times 10^{-3} \text{ m}^2 \text{ s}^{-1}$  in boreal summer while they tend to be a bit smaller in boreal winter (their Figs. 10 and 11). Based on the results of Rio and Hernandez (2003), the friction coefficient is set to be latitude-dependent in such a way that it decreases linearly from  $20 \times 10^{-3} \text{ m}^2 \text{ s}^{-1}$  at the southern end of the domain to  $10 \times 10^{-3} \text{ m}^2 \text{ s}^{-1}$  at the equator. This choice of parametrization results in an Ekman depth in the range of 60 m at 50°S to 131 m at 5°S, which is close to the results obtained by Rio and Hernandez (2003). The wind field from the NCEP reanalysis 2 (Kanamitsu et al., 2002) is used to estimate the Ekman velocity using the equations given above. All transports in this study are derived from the adjusted geostrophic velocity after the addition of the Ekman velocity. The unit Sverdrup (Sv,  $1 \text{ Sv} = 10^6 \text{ m}^3 \text{ s}^{-1}$ ) is used for transports throughout this study.

## Appendix F. Comparisons of the velocity field with other observations

To increase the confidence in the fields of the horizontal velocity derived herein, the zonal and meridional velocities at 15 m are compared to independent estimates derived from surface drifters with a drogue centered at 15 m (available at [http://www.aoml.noaa.gov/phod/dac/dac\\_meanvel.php](http://www.aoml.noaa.gov/phod/dac/dac_meanvel.php)). The methodology used to derive the drifter data set has been described in Lumpkin and Johnson (2013). At greater depths, the velocities derived herein are compared with those published previously.

<sup>6</sup> A float in every 3° by 3° box of the world oceans within 60° of the equator is the target density of the Argo array.

Before proceeding to the comparison with the drifter data set one has to keep in mind that the drifters measure the total flow including the Ekman component while the Ekman flow has to be added to the geostrophic flow field derived herein to get the total flow as described in Appendix E. The problem is that the Ekman velocity at a given level depends significantly on the friction coefficient. Herein, this is only of concern for the direct comparison of the velocities that follows below, because the primary focus of this study is on transports in layers that are mostly at least 400 m thick.

Climatological maps for the zonal and meridional velocities show good agreements of the major features of the circulation in the South Atlantic (Fig. 13). For example, both products reveal: (1) the separation between the South Atlantic Current and the Antarctic Circumpolar Current (Fig. 13, top row); (2) the Southern South Equatorial Current heading from the tip of South Africa towards the northwest; (3) the Brazil and Malvinas Currents as well as their confluence (Fig. 13, bottom row); (4) the Zapiola Gyre centered near 45°S, 45°W; (5) the Agulhas Current System including the retroflexion and the Agulhas Return Current. The main differences between the two products can be seen near the zonal boundaries and in highly dynamic regions with large mesoscale variability. In the boundary regions, relatively few observations are collected by Argo floats, which reduces the ability to fully resolve the boundary currents. In addition, the Ekman velocity at 15 m in the trade winds regime near the western boundary is strong enough to weaken the flow in the North Brazil Current significantly. However, this would not be of major concern in a study of the transport of this current because in this case the vertical integration limits would be from the surface to 200 m or more and one would get a strong transport towards the equator (Fig. 2). In the regions with large mesoscale variability, the new 3-dimensional velocity field is likely to generate a more realistic velocity field, due to the use of the sea surface height from AVISO, which resolves mesoscale features better than the array of surface

drifters can. Overall, the good agreement between the two products shows that both the methods to derive the absolute geostrophic flow described in Appendix C as well as the approach used to derive the Ekman velocities described in Appendix E work well in the study region.

At greater depths, comparisons that go beyond those of the layer transports which are studied in this paper also show good agreements of the newly derived flow field. Several examples for this are given in the following. At the western boundary Vivier and Provost (1999) published observations of the Malvinas Current based on current meters. At about 1000 m they found that the mean velocity at three mooring sites is in the range of 12.4–21.5  $\text{cm s}^{-1}$  (21.5  $\text{cm s}^{-1}$ , current meter C53 at 912 m; 16.0  $\text{cm s}^{-1}$ , current meter C63 at 1010 m; 12.4  $\text{cm s}^{-1}$ , current meter C73 at 976 m). The 1000 dbar velocities in the Malvinas Current from the new product fall into this range. For the Brazil Current, Núñez-Riboni et al. (2005) reported that the speed at intermediate depth is  $11.6 \pm 7.4 \text{ cm s}^{-1}$  south of 30°S. Plate 2 in Boebel et al. (1999) shows similar southwestward speeds in the Brazil Current between 30°S and 35°S. In this region, the velocity field derived herein has a slightly lower speed of  $9 \pm 5 \text{ cm s}^{-1}$  than what was reported by Núñez-Riboni et al. (2005). All these estimates are consistent with each other.

Proceeding to the east, Fig. 1 of Giulivi and Gordon (2006) shows the meander of the Agulhas Return Current at a location that is consistent with its location in the new velocity field derived herein. In addition to that, a study of Boebel et al. (2003) showed that the mean intermediate depth velocities in the Agulhas Current are typically about 25  $\text{cm s}^{-1}$  while those in the Agulhas Return Current are about 10  $\text{cm s}^{-1}$  (Fig. 11 in Boebel et al., 2003). Núñez-Riboni et al. (2005) reported a very similar value of  $25.3 \pm 14.2 \text{ cm s}^{-1}$  for the Agulhas Current and a larger velocity ( $22.9 \pm 13.2 \text{ cm s}^{-1}$ ) for the Agulhas Return Current. The corresponding estimates derived herein are  $28 \pm 13 \text{ cm s}^{-1}$  for the Agulhas Current and  $12 \pm 4 \text{ cm s}^{-1}$  for the Agulhas Return Current, both of which agree well with the

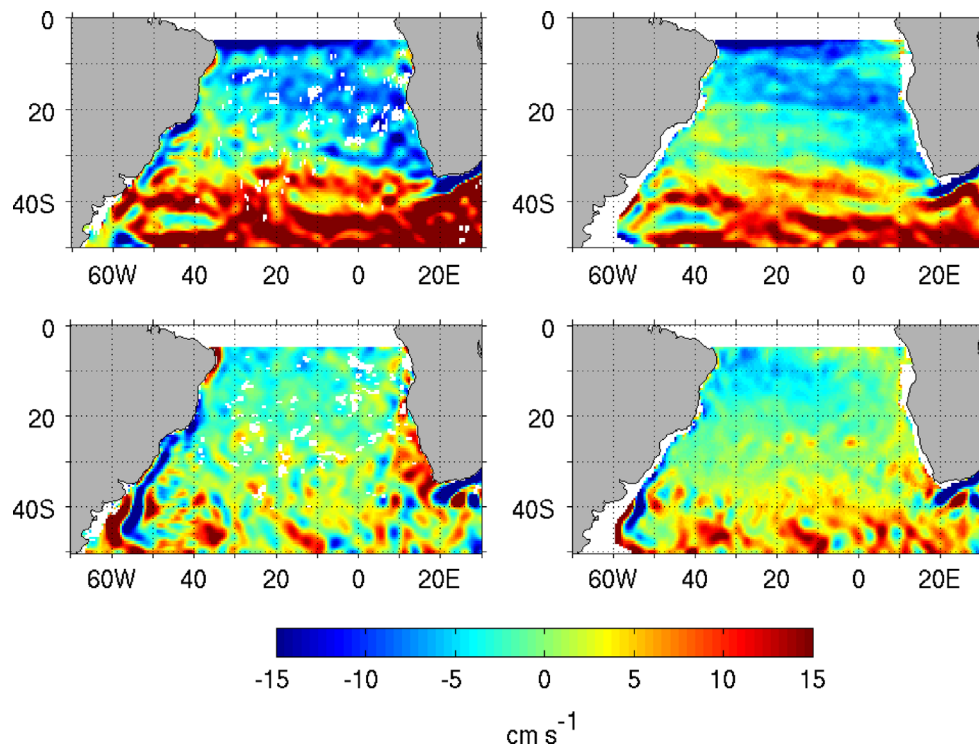


**Fig. 13.** Comparison of climatological mean of the 15 m velocities from drifters (left) with the 15 m velocities from the three-dimensional velocity field (right). The Ekman velocity is included in all panels. Top: zonal velocity. Bottom: meridional velocity. (For interpretation of the references to color in this figure caption in black-and-white copies, the reader is referred to the web version of this paper.)

results of Boebel et al. (2003). The new estimate of the Agulhas Current velocity also agrees well with the velocity derived by Núñez-Riboni et al. (2005). Given the uncertainties of the velocity estimates the difference between the velocity of the Agulhas Return Current published by Núñez-Riboni et al. (2005) and those obtained herein, as well as by Boebel et al. (2003) can be seen as insignificant.

## References

- Antonov, J.I., Locarnini, R.A., Boyer, T.P., Mishonov, A.V., Garcia, H.E., 2006. World Ocean Atlas 2005. In: Levitus, S. (Ed.), Salinity. NOAA Atlas NESDIS 62, vol. 2. U.S. Government Printing Office, Washington, DC.
- Baringer, M.O., Garzoli, S.L., 2007. Meridional heat transport determined with expendable bathythermographs. Part I. Error estimates from model and hydrographic data. *Deep-Sea Res.* 54 (8), 1390–1401.
- Benguela Current Large Marine Ecosystem Programme, 2007. In: The Changing State of the Benguela Current Large Marine Ecosystem: Expert Workshop on Climate Change and Variability and Impacts Thereof in the BCLME Region. Benguela Current Large Marine Ecosystem Programme, 15–16 May 2007.
- Bianchi, A., Garzoli, S.L., 1997. Variability and motion of the Brazil–Malvinas front. *Geoaeta* 22, 74–90.
- Boebel, O., Davis, R.E., Ollitraul, M., Peterson, R.G., Richardson, P.L., Schmid, C., Zenk, W., 1999. The intermediate depth circulation of the Western South Atlantic. *Geophys. Res. Lett.* 26 (21), 3329–3332.
- Boebel, O., Lutjeharms, J.R.E., Schmid, C., Zenk, W., Rossby, T., Barron, C., 2003. The Cape Caudron: a regime of turbulent inter-ocean exchange. *Deep-Sea Res.* II 50 (1), 57–86.
- Chapman, P., Shannon, L.V., 1985. The Benguela ecosystem. Part II. Chemistry and related processes. *Oceanogr. Mar. Biol.: Annu. Rev.* 23, 183–251.
- CLS, 1996. AVISO User Handbook for Merged TOPEX/POSEIDON products. CLS. Ref: AVI-NT-02-101.
- Davis, R.E., Webb, D.C., Regier, L.A., Dufour, J., 1992. The autonomous Lagrangian current explorer. *J. Atmos. Ocean. Technol.* 9 (6), 264–285.
- Deacon, G.E.R., 1982. Physical and biological zonation in the Southern Ocean. *Deep-Sea Res.* 29 (1), 1–15.
- Dewar, W.K., 1998. Topography and barotropic transport control by bottom friction. *J. Mar. Res.* 56, 295–328.
- Duncombe Rae, C.M., 2005. A demonstration of the hydrographic partition of the Benguela upwelling ecosystem at 26 degree 40'S. *Afr. J. Mar. Sci.* 27 (3), 617–628.
- Ekman, V.W., 1905. On the influence of the Earth's rotation on ocean-currents. *Ark. Math. Astron. Fys.* 2 (11), 1–53.
- Evans, D.L., Signorini, S.R., Miranda, L.B., 1983. A note on the transport of the Brazil Current. *J. Phys. Oceanogr.* 13, 32–37.
- Garzoli, S.L., 1993. Geostrophic velocity and transport variability in the Brazil/Malvinas Confluence. *Deep-Sea Res.* 40, 1379–1404.
- Garzoli, S.L., Baringer, M.O., 2007. Meridional heat transport determined with expendable bathythermographs. Part II. South Atlantic transport. *Deep-Sea Res.* 54 (8), 1402–1420.
- Garzoli, S.L., Baringer, M.O., Dong, S., a, R.C.P., Yao, Q., 2012. South Atlantic meridional fluxes. *Deep-Sea Res.* I 71, 21–32, <http://dx.doi.org/10.1016/j.dsr.2012.09.003>.
- Garzoli, S.L., Gordon, A.L., 1996. Origins and variability of the Benguela Current. *J. Geophys. Res.* 101 (1), 897–906.
- Georgi, D.T., 1979. Modal properties of Antarctic Intermediate Water in the south-east Pacific and the South Atlantic. *J. Phys. Oceanogr.* 9, 456–468.
- Giulivi, C.F., Gordon, A.L., 2006. Isopycnal displacements within the Cape Basin thermocline as revealed by the hydrographic data archive. *Deep-Sea Res.* 53 (8), 1285–1300, <http://dx.doi.org/10.1016/j.dsr.2006.05.011>.
- Gonzalez-Silvera, A., Santamaria-del-Angel, E., Millán-Núñez, R., 2006. Spatial and temporal variability of the Brazil–Malvinas Confluence and the La Plata Plume as seen by SeaWiFS and AVHRR imagery. *J. Geophys. Res.* 111 (C06010), 1–17, <http://dx.doi.org/10.1029/2004JC002745>.
- Gordon, A.L., 1985. Indian-Atlantic transfer of thermocline water at the Agulhas retroflection. *Science* 227, 1030–1033.
- Gordon, A.L., 1986. Interocean exchange of thermocline water. *J. Geophys. Res.* 91 (C4), 5037–5046.
- Gordon, A.L., 1989. Brazil–Malvinas Confluence – 1984. *Deep-Sea Res.* 36, 359–384.
- Gordon, A.L., Bosley, K.T., 1991. Cyclonic gyre in the tropical South Atlantic. *Deep-Sea Res.* 38 (Suppl.), 323–343.
- Gordon, A.L., Greengrove, L.C., 1986. Geostrophic circulation of the Brazil–Falkland confluence. *Deep-Sea Res.* 33 (5), 573–585.
- Gordon, A.L., Weiss, R.F., Smethie, W.M., Warner, M.J., 1992. Thermocline and intermediate water communication between the South Atlantic and Indian Oceans. *J. Geophys. Res.* 97 (C5), 7223–7240.
- Hiller, W., Käse, R.H., 1983. Objective analysis of hydrographic data sets from mesoscale surveys. *Ber. Inst. Meeresk. Univ. Kiel* 116, 78.
- Hobbs, W.R., Willis, J.K., 2012. Midlatitude North Atlantic heat transport: a time series based on satellite and drifter data. *J. Geophys. Res.* 117 (C01008), 1–14, <http://dx.doi.org/10.1029/2011JC007039>.
- Kanamitsu, M., Ebisuzaki, W., Woollen, J., Yang, S.-K., Hnilo, J., Fiorino, M., Potter, G.L., 2002. NCEP-DEO AMIP-II reanalysis (R-2). *Bull. Am. Meteorol. Soc.* 83 (11), 1631–1643.
- Lass, H.U., Mohrholz, V., 2008. On the interaction between the subtropical gyre and the Subtropical Cell on the shelf of the SE Atlantic. *J. Mar. Syst.* 74, 1–43, <http://dx.doi.org/10.1016/j.jmarsys.2007.09.008>.
- Locarnini, R.A., Mishonov, A.V., Antonov, J.I., Boyer, T.P., Garcia, H.E., 2006. World Ocean Atlas 2005. In: Levitus, S. (Ed.), Temperature. NOAA Atlas NESDIS 61, vol. 1. U.S. Government Printing Office, Washington, DC.
- Lumpkin, R., Garzoli, S.L., 2011. Interannual to decadal variability in the South-western Atlantic's surface circulation. *J. Geophys. Res.* 116 (C01014), <http://dx.doi.org/10.1029/2010JC006285>.
- Lumpkin, R., Johnson, G.C., 2013. Global ocean surface velocities from drifters: mean, variance, ENSO response, and seasonal cycle. *J. Geophys. Res.* 118 (C6), 2992–3006, <http://dx.doi.org/10.1002/jgrc.20210>.
- Lutjeharms, J.R.E., Cooper, J., 1996. Interbasin leakage through Agulhas Current filaments. *Deep-Sea Res.* 43, 213–238.
- Lutjeharms, J.R.E., Gordon, A.L., 1987. Shedding of an Agulhas Ring observed at sea. *Nature* 325, 138–140.
- McCartney, M.S., 1977. Subantarctic mode water. In: Angel, M. (Ed.), *A voyage of Discovery*, pp. 103–119.
- Núñez-Riboni, I., Boebel, O., Ollitraul, M., You, Y., Richardson, P.L., Davis, R., 2005. Lagrangian circulation of Antarctic Intermediate Water in the subtropical South Atlantic. *Deep-Sea Res.* 52, 545–564.
- Peterson, R.G., Stramma, L., 1991. Upper-level circulation in the South Atlantic Ocean. *Prog. Oceanogr.* 26, 1–73.
- Piola, A.R., Georgi, A.L., 1982. Circumpolar properties of Antarctic Intermediate Water and Subantarctic Mode Water. *Deep-Sea Res.* 29 (6A), 687–711.
- Reid, J.L., 1989. On the total geostrophic circulation of the South Atlantic Ocean: flow patterns, tracers and transports. *Prog. Oceanogr.* 23, 149–244.
- Reid, J.L., 1994. On the total geostrophic circulation of the North Atlantic Ocean: flow patterns, tracers and transports. *Prog. Oceanogr.* 33, 1–92.
- Richardson, P.L., Garzoli, S.L., 2003. Characteristics of intermediate water flow in the Benguela Current as measured with RAFOS floats. *Deep-Sea Res.* II 50 (1), 87–118.
- Rintoul, S.R., 1991. South Atlantic interbasin exchange. *J. Geophys. Res.* 96 (C2), 2675–2692.
- Rio, M.-H., Hernandez, F., 2003. High-frequency response of wind-driven currents measured by drifting buoys and altimetry over the world ocean. *J. Geophys. Res.* 108 (C8), 39/1–39/19, <http://dx.doi.org/10.1029/2002JC001655>.
- Rodrigues, R.R., Rothstein, L.M., Wimbush, M., 2007. Seasonal variability of the South Equatorial Current Bifurcation in the Atlantic Ocean: a numerical study. *J. Phys. Oceanogr.* 37 (1), 16–30.
- Rodrigues, R.R., Wimbush, M., Watts, D.R., Rothstein, L.M., Ollitraul, M., 2010. South Atlantic mass transports obtained from subsurface float and hydrographic data. *J. Mar. Res.* 68, 819–850.
- Saha, S., Nadiga, S., Thiaw, C., Wang, J., Wang, W., Zhang, Q., van den Dool, H.M., Pan, K.-L., Moorthi, S., Behringer, D., Stokes, D., White, G., Lord, S., Ebisuzaki, W., Peng, P., Xie, P., 2005. The NCEP climate forecast system. *J. Clim.* 19, 3483–3517, <http://dx.doi.org/10.1175/JCLI3812.1>.
- Schmid, C., Garraffo, Z.D., Johns, E., Garzoli, S.L., 2003. Pathways and variability at intermediate depths in the Tropical Atlantic. In: Goni, G.J., Malanotte-Rizzoli, P. (Eds.), *Interhemispheric Water Exchange in the Atlantic Ocean*, Elsevier Oceanography Series, vol. 68. Elsevier, New York, pp. 233–268.
- Schmid, C., Garzoli, S.L., 2009. New observations of the spreading and variability of the Antarctic Intermediate Water in the Atlantic. *J. Mar. Res.* 67 (6), 815–843, <http://dx.doi.org/10.1357/002224009792006151>.
- Schmid, C., Molinari, R.L., Garzoli, S.L., 2001. New observations of the intermediate depth circulation in the Tropical Atlantic. *J. Mar. Res.* 59 (3), 281–312.
- Schmid, C., Molinari, R.L., Sabina, R., Daneshzadeh, Y.-H., Xia, X., Forteza, E., Yang, H., 2007. The real-time data management system for Argo profiling float observations. *J. Atmos. Ocean. Technol.* 24 (9), 1608–1628, <http://dx.doi.org/10.1175/JTECH2070.1>.
- Schmid, C., Siedler, G., Zenk, W., 2000. Dynamics of intermediate water circulation in the Subtropical South Atlantic. *J. Phys. Oceanogr.* 30 (12), 3191–3211.
- Schmitz, W.J., 1995. On the interbasin scale thermohaline circulation. *Rev. Geophys.* 33 (2), 151–173.
- Shillington, F.A., Reason, C.J.C., Duncombe-Raeand, C.M., Florenchie, P., Penven, P., 2006. Large scale physical variability of the Benguela Current large marine ecosystem (BCLME). In: Shannon, V., Hempel, G., Malanotte-Rizzoli, P., Moloney, C.L., Woods, J. (Eds.), *Benguela*, vol. 14. Elsevier, Amsterdam, pp. 49–70.
- Sloyan, B.M., Rintoul, S.R., 2001. The Southern Ocean limb of the global deep overturning circulation. *J. Phys. Oceanogr.* 31, 143–173.
- Smythe-Wright, D., Chapman, P., Rae, C.D., Shannon, L.V., Boswell, S.M., 1998. Characteristics of the South Atlantic subtropical frontal zone between 15°W and 5°E. *Deep-Sea Res.* 45 (1), 167–192.
- Stramma, L., 1989. The Brazil Current transport south of 23S. *Deep-Sea Res.* 36, 639–646.
- Stramma, L., England, M., 1999. On the water masses and mean circulation of the South Atlantic Ocean. *J. Geophys. Res.* 104 (C9), 20863–20883.
- Stramma, L., Peterson, R.G., 1989. Geostrophic transport in the Benguela Current Region. *J. Phys. Oceanogr.* 19, 1440–1448.
- Stramma, L., Peterson, R.G., 1990. The South Atlantic Current. *J. Phys. Oceanogr.* 20, 846–859.
- Stramma, L., Schott, F.A., 1999. The mean flow field of the tropical Atlantic Ocean. In: Zenk, W., Peterson, R.G., Lutjeharms, J.R.E. (Eds.), *New Views of the Atlantic*, *Deep-Sea Res.* II 46(1–2), 279–303.
- Veitch, J., Penven, P., Shillington, F., 2010. Modeling equilibrium dynamics of the Benguela Current System. *J. Phys. Oceanogr.* 40 (9), 1942–1963, <http://dx.doi.org/10.1357/002224009792006151>.

- Vianna, M.L., Menezes, V.V., 2011. Double-celled subtropical gyre in the South Atlantic Ocean: means, trends, and interannual changes. *J. Geophys. Res.* 116 (C03024), 1–19, <http://dx.doi.org/10.1029/2010JC006574>.
- Vivier, F., Provost, C., 1999. Direct velocity measurements in the Malvinas Current. *J. Geophys. Res.* 104 (C9), 21083–21103.
- Volkov, D.L., Fu, L.-L., 2008. The role of vorticity fluxes in the dynamics of the Zapiola Anticyclone. *J. Geophys. Res.* 113 (C11015), 1–10, <http://dx.doi.org/10.1029/2008JC004841>.
- Willis, J.K., 2010. Can in situ floats and satellite altimeters detect long-term changes in Atlantic Ocean overturning? *J. Geophys. Res.* 37 (L06602), 1–5, <http://dx.doi.org/10.1029/2010GL042372>.
- Zemba, J.C., 1991. The Structure and Transport of the Brazil Current Between 27° and 36° South (Ph.D. Thesis). Woods Hole Oceanographic Institution.